# CHAPTER - 4

# Mixed metal oxide nanoparticles

## 4.1. CuO–ZnO mixed metal oxide nanoparticles

### 4.1.1. Introduction

Mixed metal oxide nanoparticles are produced by mixing two or more metal oxides through chemical or physical methods. These show a novel set of physicochemical properties that are completely changed from that of the individual metal oxides [Rodriguez and Stacchiola (2010), Nakka *et al.* (2009)]. Mixed metal oxide nanoparticles are used as heterogeneous catalysts for various important organic reactions such as reduction of aromatic nitrocompounds, cross-aldol condensation, synthesis of 1, 5-benzodiazepines and N-benzyloxycarbonylation of amines [Bayal and Jeevanandam (2012a), Gawande *et al.* (2011)]. Some mixed metal oxide nanoparticles also exhibit antibacterial activity. For example, Hassan *et al.* (2012) and Talebian *et al.* (2011) have reported antibacterial activity of $CeO_3$–$TiO_2$ and ZnO–$SnO_2$ nanoparticles against *Staphylococcus aureus*, *Salmonella typhimurium and Escherichia coli*. Mixed metal oxide nanoparticles have been synthesized in different morphologies, such as nanorods [Hassan *et al.* (2013)], nanowires [Li *et al.* (2006)], hollow nanospheres [Park *et al.* (2009)], nanosheets [Wang *et al.* (2003)], nanoplates [Zhao *et al.* (2012)] and nanocubes [Xu and Zeng (2003)]. Nanocrystalline CuO–ZnO mixed metal oxide possesses significant applications in a variety of fields and scientific areas such as water gas shift reaction [Maluf *et al.* (2010), Gines *et al.* (1995)], gas sensors [Huang *et al.* (2013)], photocatalysts [Sathishkumar *et al.* (2011)] and as catalyst for methanol preparation [Kniep *et al*. (2005), Khassin *et al*. (2013)].

ZnO is an n-type semiconductor with a wide band gap (Eg = 3.4 eV) while CuO is a p-type semiconductor with a narrow band gap (Eg = 1.2 eV) and non-toxic and easily available [Huang *et al*. (2013)]. CuO–ZnO mixed metal oxide nanoparticles show more efficient photocatalysis than that of the individual ZnO because they reduce the recombination of electrons and holes [Witoon *et al.* (2013)]. CuO–ZnO mixed metal oxide nanoparticles were used as a catalyst for the oxidation of carbon monoxide [Taylor *et al*. (2003)].

Mixed metal oxide nanoparticles have been synthesized by various methods such as solution combustion [Witoon *et al.* (2013)], solvothermal [He *et al.* (2004)], thermal decomposition [Zhao *et al.* (2010)], hydrothermal [Li *et al*. (2012)], inverse microemulsion [Gan *et al.* (1996)], electrospinnig [Yuan *et al.* (2012)], microwave irradiation [Li *et al.* (2013)], liquid-feed flame spray pyrolysis [Azurdia *et al.* (2006)], co-precipitation [Ngamcharussrivichai *et al*. (2008)], glycolysis [Imran *et al.* (2013)] and sol-gel method [Cui *et al.* (2005)]. These methods are costly as well as require sophisticated apparatus. The major drawbacks of the high temperature method, co-precipitation and others are that the products obtained, generally, possess inhomogeneity, lack of stoichiometry control and low surface area [Wei and Chen (2006)]. Particle size and shape, specific surface area, porosity and homogeneity of the mixed metal oxide nanoparticles, obtained in homogeneous precipitation method, depend on concentration of the reagents, aging time and calcination temperature of the precursors [Subrt *et al.* (2006)]. Compared to other methods, homogeneous precipitation process is a useful and attractive technique for the synthesis of nanocrystalline mixed metal oxide powder because of its significance in providing easy control of particles size and shapes [Huber *et al.* (2008), Soler-Illia *et al*. (1997), Srikanth and Jeevanandam (2009)]. The wet chemical method used by Sathiskumar *et al.* (2011) and solution combustion method by Witoon *et*

*al.* (2013) required high calcination temperature (550 $^{o}$C and 723 $^{o}$C, respectively) for the synthesis of CuO–ZnO nanoparticles. In the current work, pure nanocrystalline CuO–ZnO mixed metal oxide has been prepared for the first time by homogeneous precipitation method at low calcination temperature (350 $^{o}$C) without using any surfactant or chelating agents. This method is most promising being simple, low cost, safe and environmental friendly for the large-scale production of nanocrystalline mixed metal oxide powders. The nanocrystalline CuO–ZnO mixed metal oxide powder has also been explored as catalyst for reduction of 4-nitrophenol to 4-aminophenol using $NaBH_4$.

### 4.1.2. Experimental

(i) Materials

Copper acetate (MERCK®), zinc acetate (SRL®), ammonia solution (25%, RANKEM®), 4-nitrophenol (SRL®), $NaBH_4$ (HIMEDIA®), and Millipore® water were used as reagents as received without further purification.

(ii) Synthesis

In the present study, nanocrystalline CuO–ZnO mixed metal oxide powder was prepared using proper precursors by homogeneous precipitation method. The details of procedure are as follows.

80 mL aqueous solution of copper acetate (7 mmol) and 80 mL aqueous solution of zinc acetate (7 mmol) were taken in a 250 mL beaker. To this 10 mL of 25% ammonia solution (ammonium hydroxide) was added and the solution was heated to ~ 80 $^{o}$C with continuous stirring for 2 h. During the reaction, a brown precipitate formed, which was filtered off, washed with water several times to remove the impurities and then dried at 80 $^{o}$C in an oven. The as-prepared powder was calcined in air at 350 $^{o}$C for 2 h inside a muffle furnace (Heating rate = 1 $^{o}$C/min). The colors of the samples before and after calcination were brown and black respectively.

For the synthesis of individual CuO and ZnO powders, homogeneous precipitation reactions were carried out using 80 mL aqueous solution of either copper acetate (7 mmol) or zinc acetate (7 mmol) in a beaker and 10 mL of 25% ammonia solution was added to it. The contents were stirred at ~ 80 $^{o}$C for 2h. The rest processes were repeated as described for CuO–ZnO mixed metal oxide. The individual colors of CuO and ZnO were black and white respectively before and after calcination.

(iii) Catalytic activity test

Catalytic reactivity of the synthesized samples was determined by the reduction of 4-nitrophenol at room temperature. This reaction was also used earlier to investigate the catalytic activity of other mixed metal oxide nanoparticles [Bayal and Jeevanandam (2012a), Dhak and Pramanik (2006)]. 50 mL aqueous solution of 4-nitrophenol (4 mmol) and 50 mL of freshly prepared aqueous solution of $NaBH_4$ (0.529 mol / L) were taken in a 250 mL beaker. Then, ~ 16 mg of the catalyst (respective samples) was added to the above mixture with constant stirring at room temperature. The decolorization of the mixture indicated the complete reduction of 4-nitrophenol (yellow colored solution) to 4-aminophenol and the time taken for the same was noted.

### 4.1.3. Results and discussion

Appropriate amount of ammonium hydroxide was added to a mixture of aqueous copper acetate and aqueous zinc acetate with continuous stirring for 2 h at about 80 $^{o}$ C. This yielded CuO, copper ammonia acetate [$Cu(NH_3)_2(CH_3COO)_2$] and zinc hydroxide [$Zn(OH)_2$] (as confirmed by the XRD results). The final product CuO–ZnO mixed metal oxide particles were formed by the following reactions.

$$7Cu(CH_3COO)_2\,(aq.) + 7Zn(CH_3COO)_2\,(aq.) + 28NH_4OH\,(aq.) \rightarrow 6CuO + [Cu(NH_3)_2(CH_3COO)_2] + 7Zn(OH)_2 + 26CH_3COO^{-}\,(aq.) + 26NH_4^{+} + 8H_2O \qquad (4.1.1)$$

And the next two reactions take place during calcination at 350 $^{o}$C:

$$6CuO + 6Zn(OH)_2 \rightarrow 6CuO–ZnO + 6H_2O \quad (4.1.2)$$

$$[Cu(NH_3)_2(CH_3COO)_2] + Zn(OH)_2 \rightarrow CuO–ZnO + 2NH_3(g) + C_2H_6(g) + 2CO_2(g) + H_2(g) \quad (4.1.3)$$

The XRD data confirm the formation of pure CuO–ZnO mixed metal oxide particles after calcination at 350 $^oC$.

The powder XRD patterns of the as-prepared and calcined samples at 350 $^oC$ are shown in Figure 4.1.1. In the case of XRD pattern of the as-prepared sample there are three phases, one due to orthorhombic phase of $Zn(OH)_2$ (JCPDS file no. 38-0385), second due to copper ammonia acetate (JCPDS file no. 21-0277) and the third for monoclinic phase of CuO (JCPDS file no. 89-5895). After calcination at 350 $^oC$ diffraction peaks were observed at $2\theta \approx 34.5^o$, $36.3^o$, $47.5^o$, $56.5^o$, $62.8^o$, and $68.9^o$, which are indexed as (002), (101), (102), (110), (103), and (201) diffraction lines respectively, corresponding to hexagonal ZnO (JCPDS file no. 36-1451). In the same XRD pattern diffraction peaks of monoclinic CuO were also obtained at $2\theta \approx 54.4^o$, $65.3^o$, $66.4^o$, $67.9^o$, and $72.6^o$ which are indexed to the (020), (022), (311), (220), and (311) diffraction lines respectively (JCPDS file no. 89-5895). In the XRD pattern of the calcined sample some of the peaks of CuO have overlapped together with ZnO to give broad bands. These appear in the ranges of $31.4^o$ – $32.8^o$ and 37.5– $40.0^o$, which are indexed as (110, 100) and (111, 200) mixed diffraction lines respectively assigned for CuO–ZnO.

The diffraction peak of CuO (110) appearing at $2\theta \sim 32.73^o$ of the as-prepared sample shifts towards a lower angle ($2\theta \sim 31.83^o$) in the calcined CuO-ZnO. The shift in this peak position between the as-prepared and calcined samples is $\Delta\theta = 0.90^o$. Broadening (Full Width at Half Maxima) of the CuO (110) peak at $2\theta \sim 32.73^o$ is $0.201^o$ of the as-prepared sample and this peak merges with ZnO after calcination giving the peak (110, 100) which shows broadening (FWHM) of $0.308^o$. As a consequence it effectively changes the d-

spacings to 0.007 nm. These results suggest that $Zn(OH)_2$ and copper ammonia acetate have decomposed during calcination with the formation of hexagonal-phased ZnO and monoclinic-phased CuO.

Thus high purity nanocrystalline CuO–ZnO mixed metal oxide is formed after calcination at 350 $^oC$. The crystallite size of pure nanocrystalline CuO–ZnO mixed metal oxide was calculated using Debye-Scherrer formula. The crystallite size of ZnO is 24.7 nm and that of CuO is 16.0 nm in the mixed metal oxide.

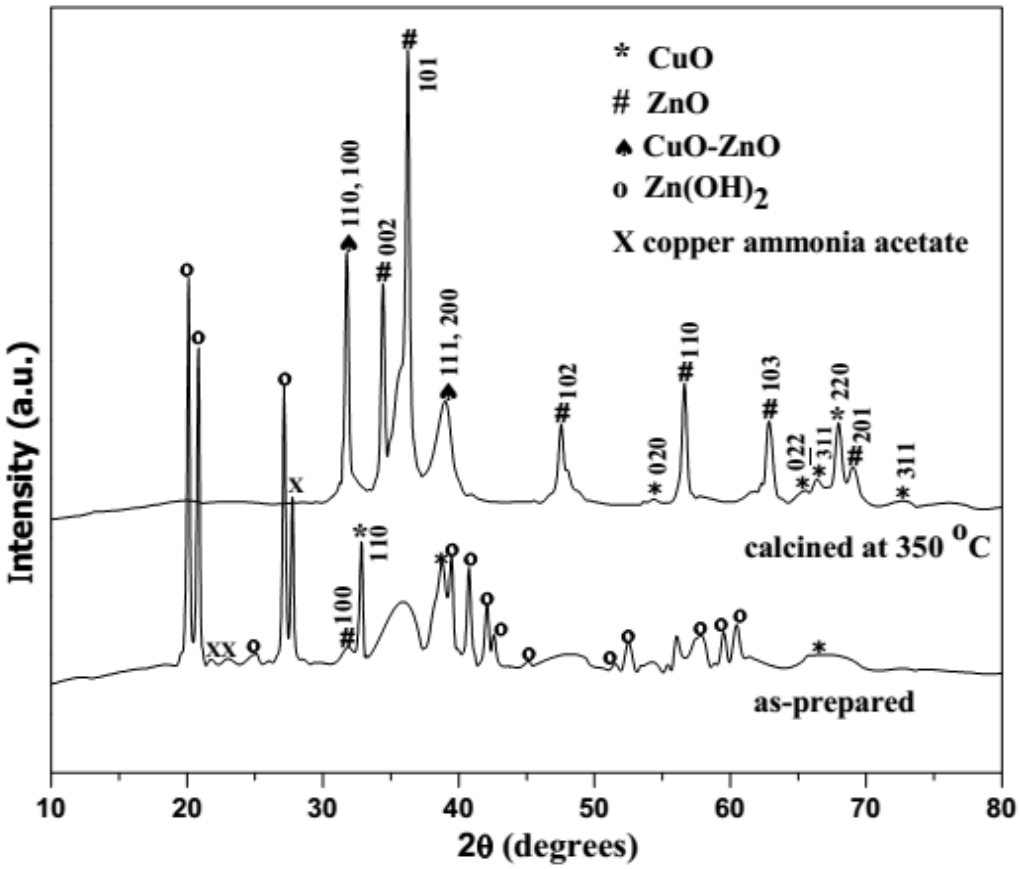


**Figure 4.1.1.** XRD patterns of as-prepared and calcined nanocrystalline CuO–ZnO mixed metal oxide.

The elemental analysis (CHN) results of as-prepared powder sample are % C = 3.36, % H = 1.82 and % N = 1.92. This confirms the presence of the components given in the reactions.

The thermal gravimetric analysis pattern of the as-prepared powder sample is shown in Figure 4.1.2. The overall weight losses (about 12 %) between 112-400 $^{o}$C are attributed to the evaporation of water and also to the removal of inorganic and organic matters obtained from the decomposition of copper ammonia acetate. There is virtually not any weight loss after 350 $^{o}$C.

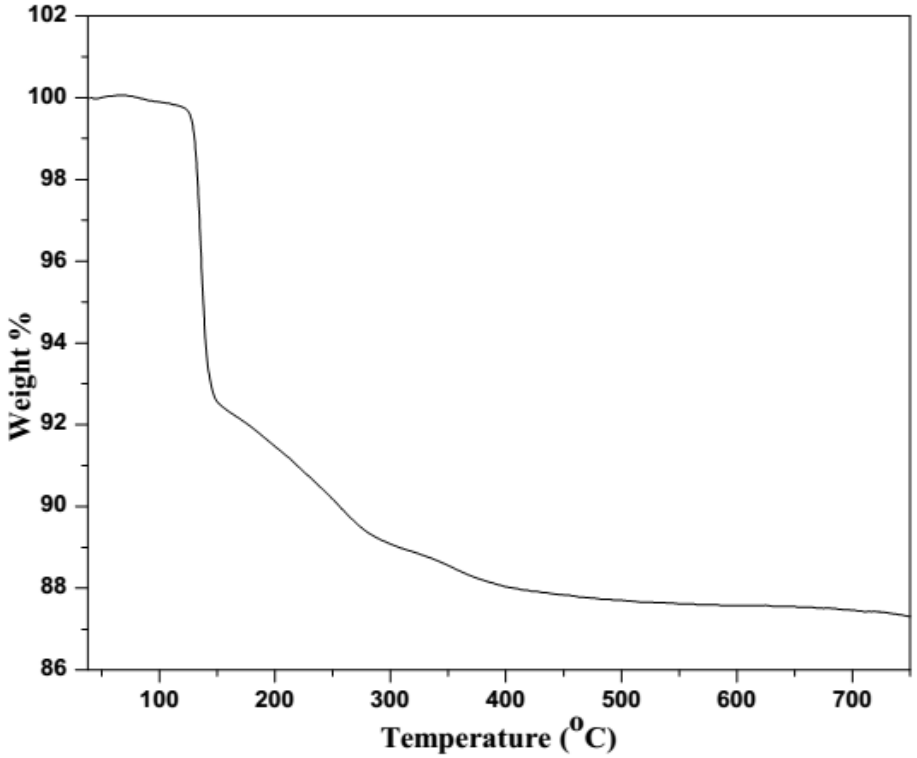


**Figure 4.1.2.** Thermal gravimetric analysis curves of as-prepared sample.

The FT-IR spectra of as-prepared and calcined CuO–ZnO mixed metal oxide samples are shown in Figure 4.1.3. The characteristic band appearing at 3232 cm$^{-1}$ in the spectra of as-prepared sample shows that nitrogen of ammonia is involved in coordination with copper (II) but it is not present in the calcined sample [Hadush *et al.* (2013)]. The broad band between 3413 and 3502 cm$^{-1}$ are due to surface-adsorbed water in the spectra of the calcined sample [Huang *et al.* (2013)]. The medium bands at about 2161, 2109, and 2048 cm$^{-1}$ of as-prepared sample are attributed to N-H stretching vibrations [Silverstein and Webster (2011)]. The band at 1780 cm$^{-1}$ is assigned to the binding of acetate ion to

copper (II) in the as-prepared sample [Hosny and Zoromba (2012)] which disappears in case of calcined sample. The bands observed between 1361-1479 $cm^{-1}$ are attributed to the C-C, δ (OH) and C-O vibrations [Khassin *et al.* (2013), Li *et al.* (2013)]. The bands at 1029 and 1090 $cm^{-1}$ appear due to symmetric stretching of O-H vibration in the as-prepared sample but these disappear in the calcined sample. The metal-oxygen stretching frequencies appearing in the range of 539-850 $cm^{-1}$ are associated with the vibrations of Cu-O and Zn-O [Erdogan (2010)]. The band occurring at 507 $cm^{-1}$ is attributed to νCu-$NH_3$ which indicates that ammonia is in coordination to Cu (II) [Hadush *et al.* (2013)]. The lower frequency band at 455 $cm^{-1}$ shows νCu-O suggesting the binding of acetate group of copper ammonia acetate in the as-prepared sample. The νCu-$NH_3$ and νCu-O (acetate) bands are absent in the spectrum of the calcined sample.

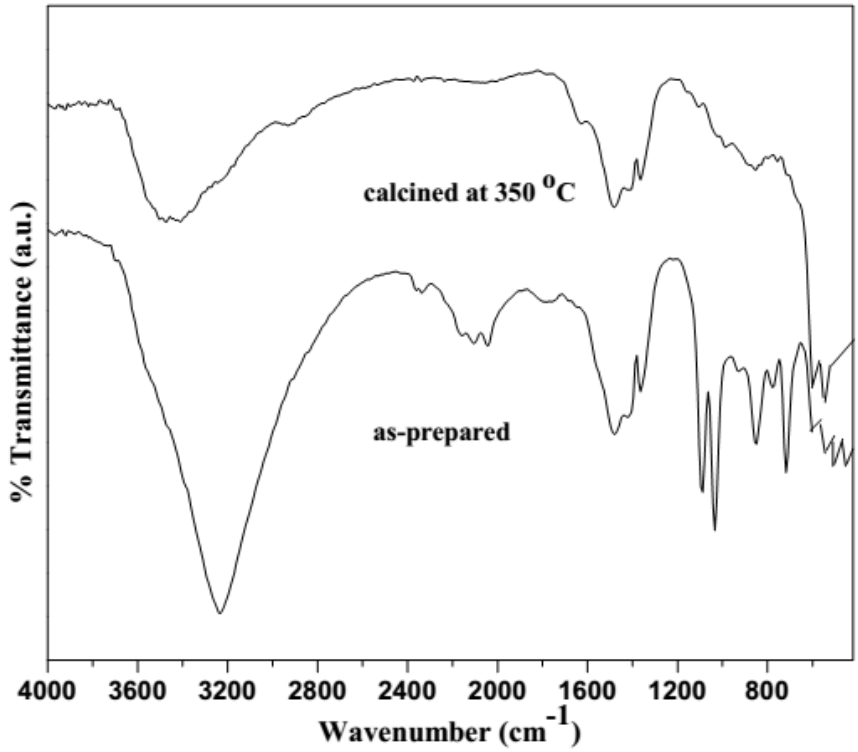


**Figure 4.1.3.** FT-IR spectra of as-prepared and calcined nanocrystalline CuO–ZnO mixed metal oxide.

Diffuse reflectance spectra of nanocrystalline samples are shown in Figure 4.1.4(a). The band gap of nanocrystalline CuO–ZnO mixed metal oxide was estimated using the following equation [Sathishkumar *et al.* (2011)] and from the extrapolation of the linear relationship between $(\alpha h\upsilon)^2$ and $h\upsilon$:

$$(\alpha h\upsilon)^2 = K(h\upsilon - E_g) \qquad (4.1.4)$$

where $\alpha$ is the absorption coefficient, K is a proportionality constant and $\upsilon$ is the frequency of photons. The $(\alpha h\upsilon)^2$ versus $h\upsilon$ is plotted in Figure 4.1.4(b) on the basis of data obtained from Figure 4.1.4(a). Nanocrystalline CuO–ZnO mixed metal oxide exhibits the absorption band gap at 3.19 eV as shown in Figure 4.1.4(b). For pure ZnO nanoparticles the absorption band gap is reported at 3.9 eV [Mashford *et al.* (2010)]. In the present case, the band gap shifts towards a lower value as it is influenced by CuO in mixed CuO-ZnO. The band gap of nanoparticles depends on the particle size, crystalline structure, compositions and the defects in the arrangement of ZnO [Sathishkumar *et al.* (2011), Erdogan (2010)].

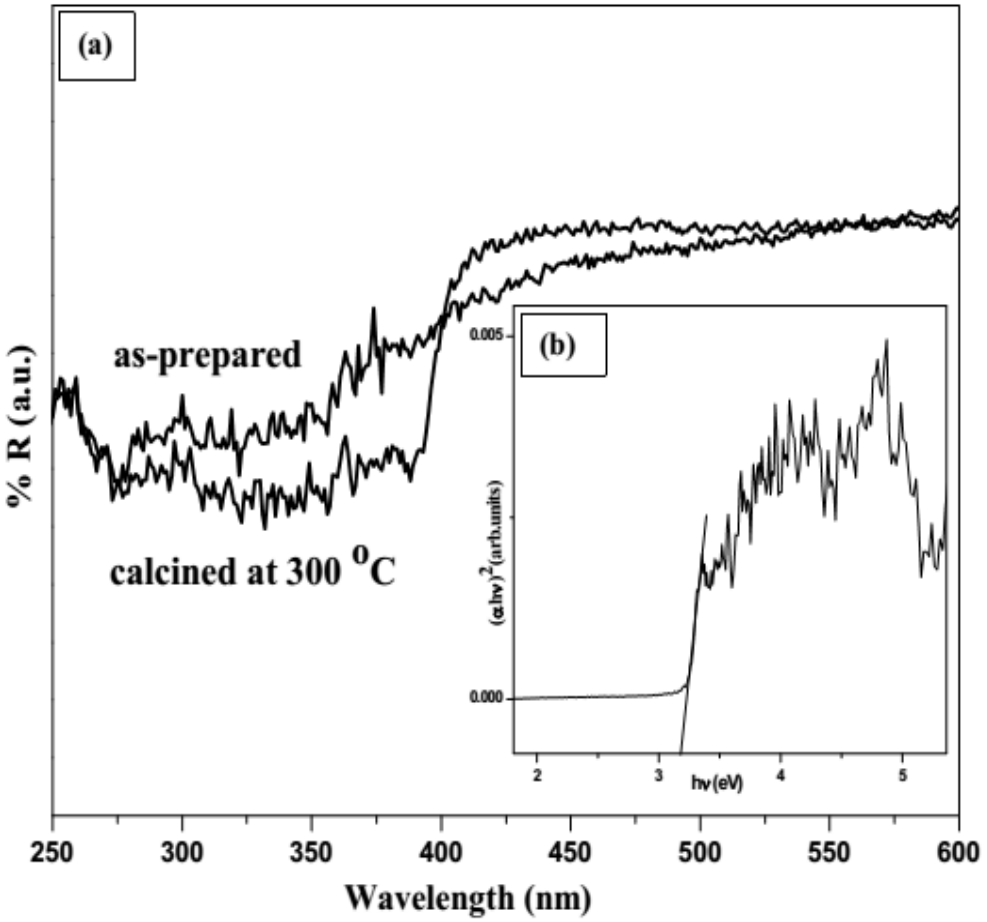


**Figure 4.1.4.** (a) Diffuse reflectance spectra of nanocrystalline CuO–ZnO mixed metal oxide, and (b) The plot of $(\alpha h\upsilon)^2$ vs. $h\upsilon$ according to the data from (a).

Surface area measurements (BET) were carried out for nanocrystalline CuO–ZnO mixed metal oxide before and after calcination. The results indicate that as-prepared sample has high specific surface area (SSA ~ 31.6 – 26.2 $m^2g^{-1}$) compared to the calcined nanocrystalline CuO–ZnO mixed metal oxide (350 $^oC$: SSA ~ 22.3 $m^2g^{-1}$). The specific surface area depends on the precipitation time of the samples (Table 4.1.1). Precipitation time was varied according to the ageing time. It is observed that as the precipitation time increases the specific surface area also increases (Table 4.1.1). This is because during the precipitation there was continuous stirring and more collisions between the particles forming these into smaller sizes. A high surface area goes along with small particle sizes. The specific surface area of CuO–ZnO mixed metal oxide synthesized by the hydrothermal method [Huang *et al.* (2013)] and wet impregnation method [Sathishkumar

*et al.* (2011)] are about 17.1 $m^2g^{-1}$ and 14.0 $m^2g^{-1}$, respectively which are lower than that of the present method.

**Table 4.1.1.** Precipitation time and BET surface area of as-prepared sample.

| **Precipitation time (min)** | **Surface area ($m^2$ $g^{-1}$)** |
|---|---|
| 60 | 26.2 |
| 90 | 29.4 |
| 120 | 31.6 |

The FE-SEM images of as-prepared and calcined nanocrystalline CuO–ZnO mixed metal oxide in different magnifications are shown in Figures 4.1.5 and 4.1.6. The FE-SEM images of as-prepared sample show rice-like structures for CuO while irregular plate-like morphology for ZnO precursor, i.e., $Zn(OH)_2$ (as confirmed by the EDXA results) (Figure 4.1.5(a) – (c)). In the calcined nanocrystalline CuO–ZnO mixed metal oxide, the rice-like particles of CuO get arranged in the form of a compact colar-like morphology, but ZnO retains its same irregular plate-like morphology (Figure 4.1.6(a) – (c)).

The EDX analysis results indicate the presence of copper, zinc and oxygen elements in the as-prepared and calcined nanocrystalline CuO–ZnO mixed metal oxide (Figure 4.1.5(d)).

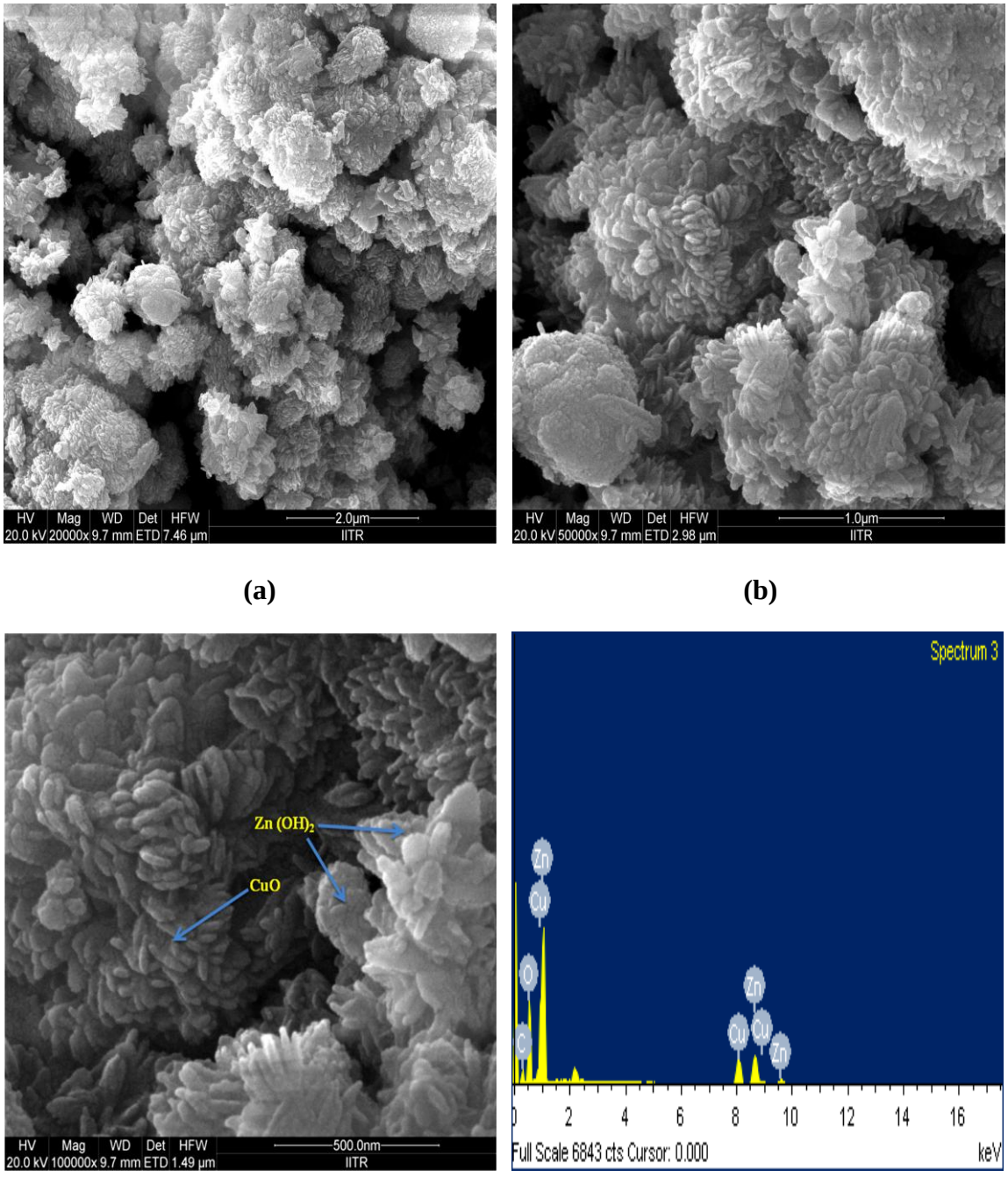


**Figure 4.1.5.** FE-SEM images of the as-prepared sample under different magnifications (a) 2µm, (b) 1µm, (c) 500 nm, and (d) EDX analysis plot of the nanocrystalline CuO–ZnO mixed metal oxide.

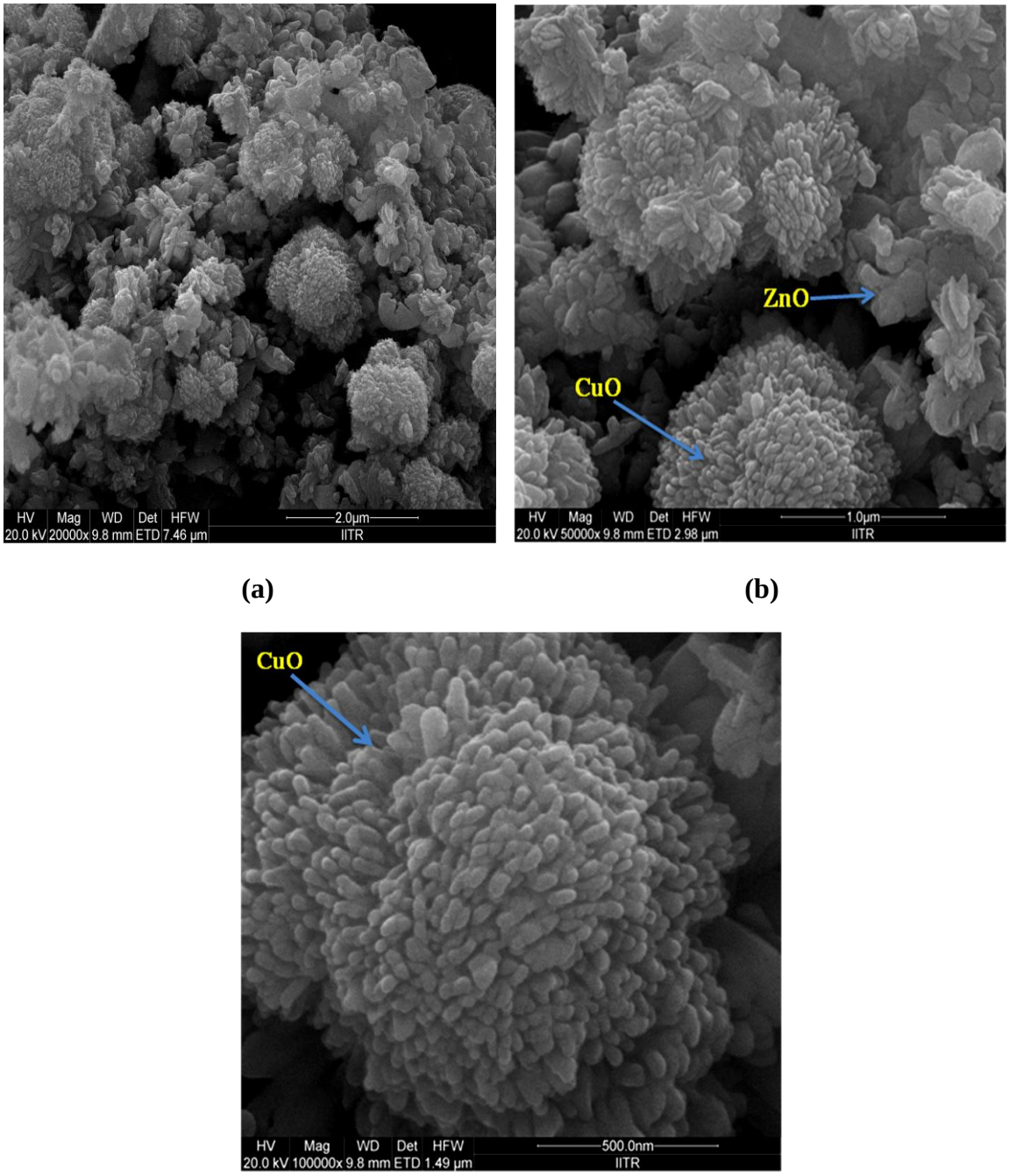


**Figure 4.1.6.** FE-SEM images of the calcined nanocrystalline CuO–ZnO mixed metal oxide under different magnifications (a) 2µm, (b) 1µm, and (c) 500 nm.

The EDX analyses show that the colar-like and irregular plate-like morphology contains Cu and Zn. The average atomic percent of Cu and Zn are ~17.9 and 2.1 respectively in the colar-like morphology, whereas in the irregular plate-like morphology the average atomic percent of Cu and Zn are ~1.9 and 16.7, respectively. EDX analyses data confirmed that colar-like and plate-like morphologies are mainly composed of CuO and ZnO particles respectively. The carbon peak in the EDX patterns is due to the carbon conducting tape used during the measurements.

Nanocrystalline CuO–ZnO mixed metal oxide powder was further investigated by typical TEM images. The TEM image (Figure 4.1.7) shows spherical particles of CuO which have aggregated in the form of rice-like structure as displayed by FE-SEM (Figure 4.1.5(a) – (c)). The average size of the spherical particles is about 18.2 ± 0.4 nm. This is in good agreement with the results of XRD having crystallite size of 16.0 nm. The irregular plate-like morphology of ZnO contains agglomerated small rod particles.

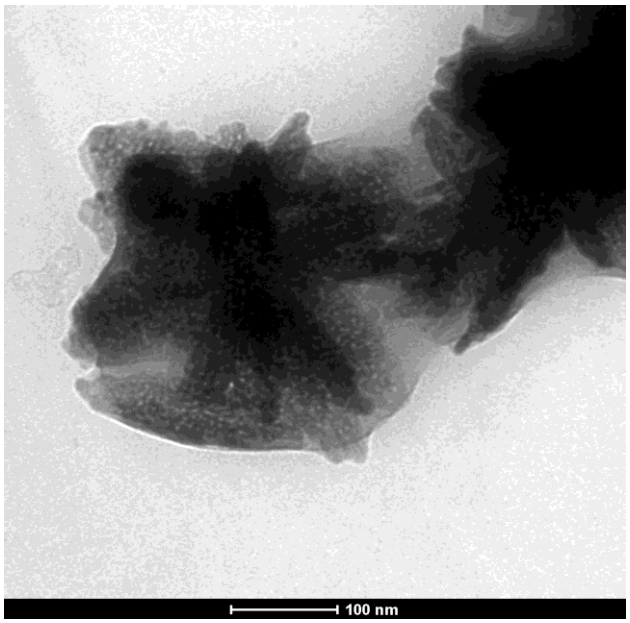


**Figure 4.1.7.** Typical TEM images of the nanocrystalline CuO–ZnO mixed metal oxide.

The catalytic activity of the synthesized samples was tested for the reduction of 4 nitrophenol (4-NP) to 4-aminophenol (4-AP) using sodium borohydride as reducing agent. The time required for the complete reduction of 4-nitrophenol to 4-aminophenol as indicated by the decolorization of yellow colour of 4-nitrophenol in the presence of synthesized samples are reported in Table 4.1.2. A blank reaction was also carried out in the absence of the catalyst. It is inferred from the Table 4.1.2 that the reduction of 4-nitrophenol does not take place either in the absence of the catalyst or using pure ZnO nanoparticles. The as-prepared sample took less time (Table 4.1.2) for the decolorization of the 4-nitrophenol solution showing that it acts as a better catalyst compared to the calcined sample as well as from pure CuO nanoparticles. The reduction of 4-nitrophenol by $NaBH_4$ in the presence of catalyst occurs in two steps [Mandlimath and Gopal (2011)]. In the first step, adsorption of 4-nitrophenolate and $BH_4^-$ ions takes place on the surface of the catalyst by chemical interaction (chemisorption). In the second step, the catalyst assists the transfer of electron from $BH_4^-$ ions (donor) to the $NO_2$ group (acceptor) to form 4-aminophenolate ions. Desorption of the 4-aminophenolate ions occurs immediately from the catalyst surface as shown in Figure 4.1.8.

**Table 4.1.2.** Time required for the complete reduction of 4-nitrophenol in the presence of different metal oxide nanoparticles as catalysts.

| S. No. | Reaction condition | Time required for the reduction (min) |
|---|---|---|
| 1. | 4-Nitrophenol + $NaBH_4$ | No reduction |
| 2. | 4-Nitrophenol + $NaBH_4$ + ZnO | No reduction |
| 3. | 4-Nitrophenol + $NaBH_4$ + CuO | 14 |
| 4. | 4-Nitrophenol + $NaBH_4$ + as-prepared sample | 6 |
| 5. | 4-Nitrophenol + $NaBH_4$ + CuO–ZnO (calcined) | 10 |

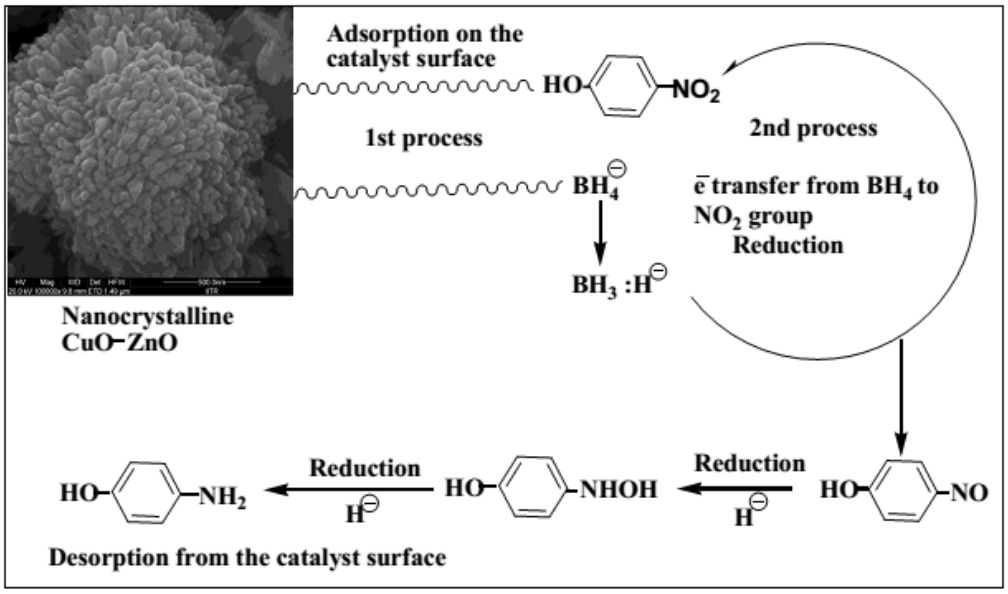


**Figure 4.1.8.** Schematic diagram indicating the mechanism for the reduction of 4-nitrophenol to 4-aminophenol in the presence of synthesized samples.

## 4.2. ZnO–NiO mixed metal oxide nanoparticles

### 4.2.1. Introduction

Mixed metal oxide nanostructures formed by the combination of p- and n-type semiconductors play a very important role for their unique physical and chemical properties which are completely different from their individual metal oxides [Liu *et al.* (2014)]. The n-type semiconductor zinc oxide (ZnO) having a wide direct band-gap (3.37 eV) and large exciton binding energy (60 meV), provides potential applications in various fields such as sensors, transparent coating for solar cells, light-emitting diodes, optoelectronic, laser devices, piezoelectric devices, catalysis, UV protection, cosmetics, paints and pharmaceuticals [Darezereshki *et al.* (2011), Tari *et al*. (2012), Jia *et al.* (2008), Tawale *et al.* (2010)]. While nano-structured nickel oxide (NiO), which is a p-type semiconductor with a stable wide band gap (3.6-4.0 eV), got extensive use in drug delivery, battery cathodes, photoelectrodes, adsorbents, photocatalysts, electrochemical capacitors, electrochromic windows and magnetic materials [Saghatforoush *et al.* (2012), Hayat *et al.* (2011), Behnajady and Bimeghdar (2014), Sun *et al.* (2014), Thota and

Kumar (2007)]. Due to the build-up of an inner electric field at the p–n junction interface the nanocrystalline ZnO–NiO mixed metal oxide has superior functional performances in comparison to the consequent single-phase metal oxides [Chen *et al.* (2012)]. It is also found [Xu *et al.* (2012)] that ZnO and NiO easily form p-n heterojunction and create an electrical barrier between crystal grains which show good sensitivity to $H_2S$ gas. In ZnO or NiO semiconductor fast recombination of photogenerated electron-hole pairs occur which is suppressed in ZnO–NiO mixed metal oxide by improving the efficiency of net charge transfer in the reaction process. Thus, it exhibits excellent photocatalytic activity for degradation of methyl orange and in sensing gas for detection of acetone [Liu *et al.* (2014)]. They are also used as more efficient photocatalysts for the hydrogen production under visible light [Belhadi *et al.* (2011)]. The physicochemical properties of the mixed metal oxide nanoparticles significantly depend on surface area, pore morphology, particle size, pore matrix-interface, porosity and the synthetic methods used for their preparation [Aslani *et al.* (2011)].

Synthesis of nanocrystalline ZnO–NiO mixed metal oxide has been done by various routes like solvothermal [Aslani *et al.* (2011)], hydrothermal [Abbasi *et al.* (2014)], solid-state reaction [Raza *et al.* (2011)], electrospinning [Dorneanu *et al.* (2014)], high energy mechanical ball milling [Kakazey *et al.* (2014)], thermal evaporation [Oboudi *et al.* (2013)], sonochemical [Rahman *et al.* (2014)] and sole-gel combustion [Zak *et al.* (2012)] methods. In its preparation the growth of controlled size nanoparticles is an intricate task. The reported methods have many drawbacks since they needed complicated equipments, high-energy, higher processing temperature and long reaction time. The homogeneous precipitation process is particularly attractive among the above methods because of its low cost, used in large-scale industrial production without utilizing expensive raw materials and sophisticated equipments. It has an easy control in the production of

uniform powders and particle size [Zhang *et al.* (2005), Soler-Illia *et al.* (1997)]. The solvothermal method used by Aslani *et al.* (2011) needed teflon-lined stainless steel autoclaves and required longer reaction time (12 h) for its synthesis and the electrospinning technique by Dorneanu *et al.* (2014) took more longer reaction time (24 h). Raza *et al.* (2011) prepared the nanoparticles by the solid-state reaction at high calcination temperature (800 °C). In the present work, pure nanocrystalline ZnO–NiO mixed metal oxide has been synthesized by the homogeneous precipitation method at low calcination temperature (350 $^{o}$C) in short time without using any surfactant or chelating agents. The method being simple, economical, environment friendly and harmless is of great potential for the large batch production of nanocrystalline mixed metal oxide powders. 4-Nitrophenol (4-NP) and its derivatives are the major sources of organic pollutants that occur in industrial waste water. They normally result from the production and consumption process of synthetic dyes, insecticides, explosive, pesticides, herbicides and agrochemicals [Feng *et al.* (2013)]. 4-Aminophenol (4-AP) is a very useful and important intermediate in the preparation of a variety of analgesic and antipyretic drugs such as paracetamol, acetaminophen, acetanilide and phenacetin [Sharma and Jeevanandam (2013)]. 4-AP is a strong reducing agent and is used as photographic developer, corrosion inhibitor in paints, anticorrosion-lubricating agent in fuels, hair-dyeing agent, wood stain etc. [Feng *et al.* (2013), Zhang *et al.* (2011)]. There are several methods for the conversion of nitrophenol to aminophenol [Mandlimath and Gopal (2011), Abbar *et al.* (2007), Polat *et al.* (2002), Du *et al.* (2004)], but the disadvantages of these methods include longer duration, wide methodology, formation of side product, serious pollution problem, corrosion of the equipment and are of expensive nature [Mandlimath and Gopal (2011)]. Hence, there is an increasing demand for an important, efficient and greener route for the direct catalytic reduction of 4-NP to 4-AP. This

encouraged the authors to synthesize an effective and better catalyst for the reduction of 4-nitrophenol to 4-aminophenol using sodium borohydride. For this purpose nanocrystalline ZnO–NiO mixed metal oxide has been prepared, characterized by different techniques and its catalytic property for the reduction of 4-NP to 4-AP has been explored.

### 4.2.2. Experimental

(i) Materials

The chemicals used were nickel (II) acetate ($Ni(CH_3COO)_2 \cdot 4H_2O$) (98%, ALDRICH®), zinc (II) acetate ($Zn(CH_3COO)_2 \cdot 2H_2O$) (MERCK®), ammonia solution (25%, RANKEM®), 4-nitrophenol (SRL®) and $NaBH_4$ (HIMEDIA®). All the chemicals were of analytical grade and used as reagents as received without further purification. The solutions were prepared in Millipore® water.

(ii) Synthesis

In the present study, nanocrystalline ZnO–NiO mixed metal oxide powders were prepared using suitable precursors by a surfactant-free homogeneous precipitation method. The synthetic details are as follows.

In a 250 mL beaker 80 mL aqueous solution of nickel acetate (6 mmol) and 80 mL aqueous solution of zinc acetate (6 mmol) were taken. Subsequently, 10 mL of 25% aqueous ammonia solution (ammonium hydroxide) was added dropwise into the above solution and the contents were heated to ~ 75 $^oC$ with continuous stirring for 2 h. During the reaction blue color of the solution disappeared and light green precipitate was obtained. Afterwards it was filtered off, washed with water many times to remove the impurities and then finally with ethyl alcohol and dried at 85 $^oC$ in an oven. The as-prepared sample was grounded to a fine powder with a mortar and pestle. Calcination of the as-prepared powder was carried out in air at 350 $^oC$ and 500 $^oC$ at a heating rate of 1

°C/min for 2 h inside a muffle furnace. The colors of the samples before and after calcination were green and black respectively.

(iii) Catalytic activity test

The catalytic ability of the synthesized nanocrystalline ZnO–NiO mixed metal oxide powders was assessed for the reduction of 4-nitrophenol (4-NP) to 4-aminophenol (4-AP) using $NaBH_4$ as reducing agent. This reaction was also used previously [Feng *et al.* (2013), Mandlimath and Gopal (2011), Bayal and Jeevanandam (2012a)] to test the catalytic reactivity of different metal oxide/mixed metal oxide nanoparticles. In a 250 mL beaker about 50 mL aqueous solution of 4-nitrophenol (0.3 mmol) and 50 mL of freshly prepared aqueous solution of $NaBH_4$ (0.53 mol/L) were taken. About 20 mg of the catalyst (prepared samples) was added into the above mixture with constant stirring at room temperature. The decolorization of the mixture indicated the complete reduction of 4-nitrophenol (yellow colored solution) to 4-aminophenol (colorless solution) and the time taken for the same was noted. A blank reaction was also carried out in the absence of the catalyst.

### 4.2.3. Results and discussion

Proper amount of ammonium hydroxide solution was added to a mixture of aqueous nickel acetate and aqueous zinc acetate with continuous stirring for 2 h at about 75 $^{o}$ C and the following reactions took place:

$$Zn(CH_3COO)_2 \bullet 2H_2O + Ni(CH_3COO)_2 \bullet 4H_2O + 4NH_4OH \rightarrow Zn(OH)_2 + Ni(OH)_2 + 4CH_3COONH_4 + 6H_2O \quad (4.2.1)$$

$$Zn(OH)_2 \rightarrow ZnO + H_2O \quad (4.2.2)$$

After calcination:

$$ZnO + Ni(OH)_2 \rightarrow ZnO–NiO + H_2O \quad (4.2.3)$$

The XRD data confirm the formation of pure nanocrystalline ZnO–NiO mixed metal oxide after calcination.

The powder XRD results of the as-prepared and calcined samples are shown in Figure 4.2.1. XRD pattern of the as-prepared sample shows peaks only due to the alpha-nickel hydroxide hydrate with a hexagonal structure ($\alpha$-$Ni(OH)_2 \bullet H_2O$) (JCPDS file no. 22-0444). Zinc oxide being amorphous does not show any XRD peak. After calcination at 350 $^oC$ and 500 $^oC$ diffraction peaks were observed at $2\theta \approx 31.7^o$, $34.3^o$, $36.3^o$, $47.5^o$, $56.5^o$, $67.9^o$ and $69.0^o$ which are indexed at diffraction lines of (100), (002), (101), (102), (110), (112) and (201) respectively corresponding to hexagonal ZnO with lattice parameters of a = 0.3250 nm and c = 0.5207 nm (JCPDS file no. 36-1451). In the same XRD pattern diffraction peaks of face-centered-cubic (fcc) structured NiO with lattice parameters of a = 0.4177 nm were also obtained at $2\theta \approx 43.1^o$, $62.7^o$, $75.2^o$ and $79.3^o$ which are indexed to the (200), (220), (311) and (222) diffraction lines respectively (JCPDS file no. 78-0429). It is observed that for the sample calcined at 500 $^oC$ an additional diffraction peak of NiO (111) appears at $2\theta \approx 37.2^o$. The XRD patterns confirm the formation of pure nanocrystalline ZnO–NiO mixed metal oxide after calcination at 350 $^oC$. The crystallite sizes of the calcined samples were calculated from the high intense diffraction peaks, i.e. (101) of ZnO and (200) of NiO using the Debye–Scherrer formula as given below:

$$D = 0.89\,\lambda / \beta \cos\theta \qquad (4.2.4)$$

where D is the crystallite size in nanometers, 0.89 represents a dimensionless constant k, $\lambda$ is the wavelength of Cu-K$\alpha$ (0.15406 nm), $\beta$ is the full width at half maximum (FWHM, radian) of prominent intensity peak (using the 100% relative intensity peak will be used) and $\theta$ is the diffraction angle (degree). The crystallite size of ZnO is 6.8 nm and that of NiO is 8.2 nm in the sample calcined at 350 $^oC$ while ZnO is 27.0 nm and that of NiO is

11.3 nm in the sample calcined at 500 $^{o}$C. These XRD analyses suggest that on increasing calcination temperature the intensity of the diffraction peaks also increase which is attributed to the larger crystallite size.

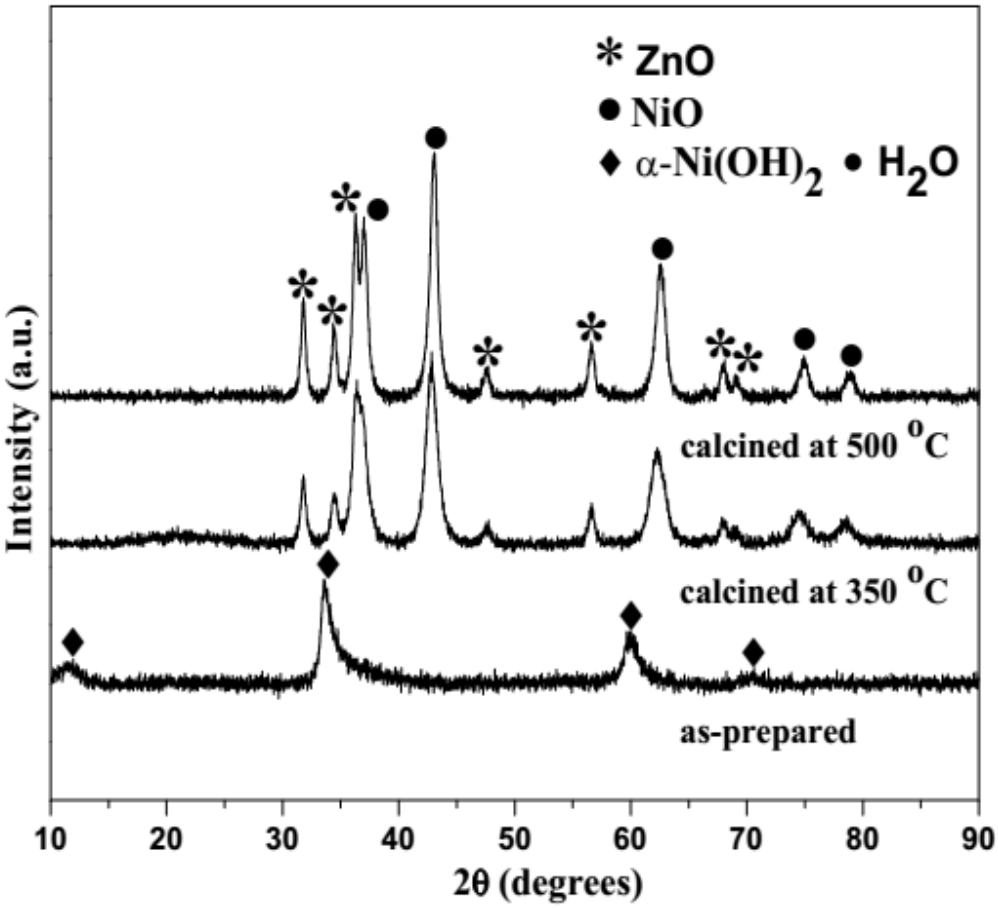


**Figure 4.2.1.** XRD patterns of as-prepared and calcined nanocrystalline ZnO–NiO mixed metal oxide.

There are two steps of weight loss in the thermal gravimetric analysis patterns for as-prepared powder as shown in Figure 4.2.2. The first weight loss step (about 7.3 mass %) is due to removal of physically absorbed water at about 170 °C [Zak *et al.* (2011)]. The second weight loss (about 18.2 mass %) in the region 170–350 $^{o}$C is associated with the removal of water from the thermal decomposition of $Ni(OH)_2$ to NiO [El-Kemaryn *et al.* (2013)]. Above 350 $^{o}$C there is no appreciable change in weight confirming the formation of pure nanocrystalline ZnO–NiO mixed metal oxide.

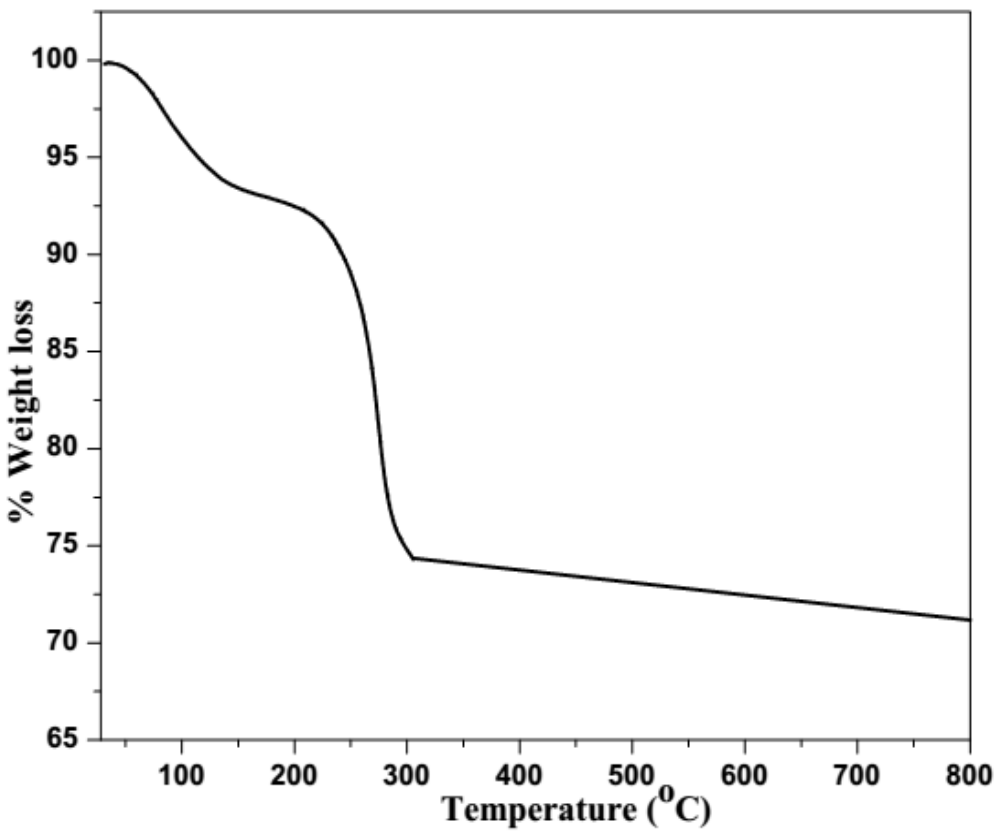


**Figure 4.2.2.** Thermal gravimetric analysis curves of as-prepared sample.

The FT-IR spectra of as-prepared and calcined samples are presented in Figure 4.2.3. The broad absorption band observed at 3526 $cm^{-1}$ corresponds to the stretching vibration of hydroxyl group (νO-H) of the absorbed water by the FT-IR sample disks prepared in open air [Christy and Umadevi (2013), Kalam *et al.* (2013)]. The absorption peaks at 1567 and 1343 $cm^{-1}$ in the spectra of as-prepared sample are assigned to the asymmetric and symmetric C=O bond vibrations respectively [Song and Gao (2008), Abbad *et al.* (2013)]. The broad band at about 652 $cm^{-1}$ in the as-prepared sample is ascribed to the stretching vibration of hydroxyl groups of the hydrogen bonded Ni–O [Kalam *et al.* (2013)]. The band at 520 $cm^{-1}$ is attributed to the Zn-O stretching vibrations in the spectra of as-prepared and calcined samples [Abbad *et al.* (2013)]. The band at 472 $cm^{-1}$ is related to the Ni–O stretching vibration of $NiO_6$ octahedral in the cubic NiO structure in the spectra of calcined samples [Al-Sehemi *et al.* (2014)].

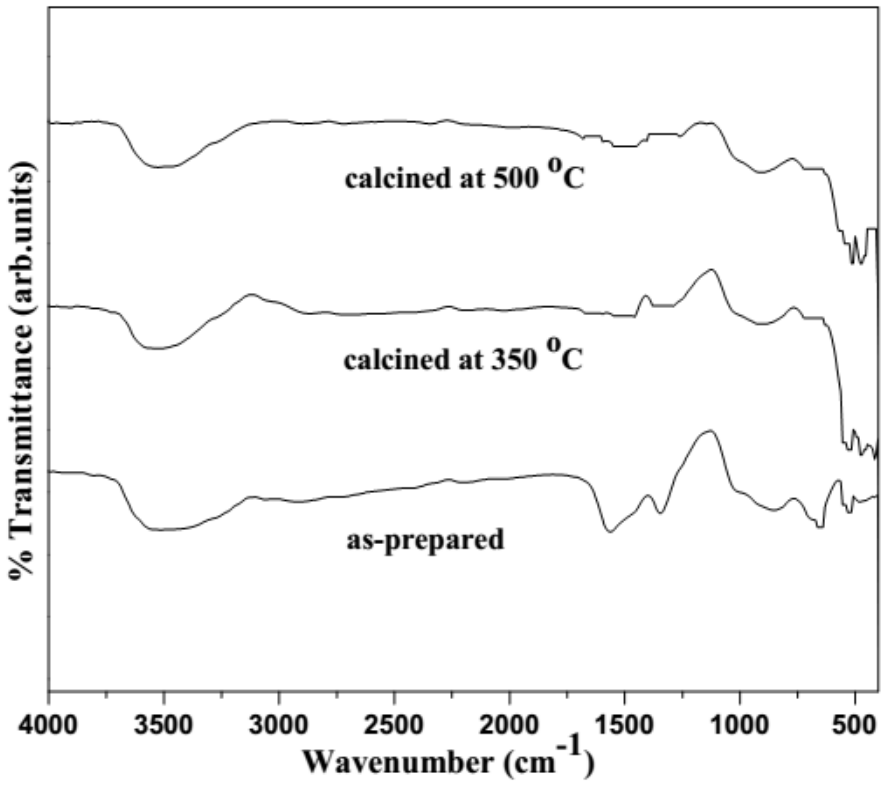


**Figure 4.2.3.** FT-IR spectra of as-prepared and calcined nanocrystalline ZnO–NiO mixed metal oxide.

UV-Visible diffuse reflectance spectroscopy is one of the extensive methods to find out the energy structures and optical properties of the semiconductor nanocrystals. Diffuse reflectance spectra of nanocrystalline ZnO–NiO mixed metal oxide calcined at 350 $^{o}$C and 500 $^{o}$C are shown in Figure 4.2.4(a). The energies of the optical band gaps (Eg) of the samples have been estimated using Kubelka-Munk model. It is used to calculate the optical absorption coefficient (α) by the measurement of the UV-Visible diffuse reflectance spectra and is mostly used for powder samples.

Kubelka-Munk function, F(R) is directly proportional to the optical absorption coefficient (α) and the value is calculated from the following equation [Manikandan *et al.* (2013)]:

$$(F(R)) = \alpha = (1- R)^2/2R \qquad (4.2.5)$$

where F(R) is the Kubelka-Munk function which equivalents to the absorbance and R is the reflectance of the sample. The optical band gap (Eg) of the nanocrystalline ZnO–NiO mixed metal oxide was determined by using Tauc relationship [Christy and Umadevi (2013), Al-Sehemi *et al.* (2014)]:

$$(\alpha h\upsilon)^n = K(h\upsilon - E_g) \qquad (4.2.6)$$

where hυ is the photon energy and K is the constant related to the transition probability of the material and n indicates either 2 or 1/2 for direct transition and indirect transition respectively [Song and Gao (2008)]. The plots between $(\alpha h\upsilon)^2$ on the y axis and photon energy (hυ) on the x-axis are given in Figures 4.2.4(c) and (d) which have been obtained from the data of Figures 4.2.4(a) and (b) respectively. The estimated band-gap energy of ZnO and NiO are 3.21 and 3.72 eV respectively for the sample calcined at 350 $^oC$, while these for the sample calcined at 500 $^oC$ are 3.16 and 3.68 eV for ZnO and NiO respectively [Kakazey *et al.* (2014)]. Hence, with the increase of the calcination temperature or crystallite size of the nanocrystalline ZnO–NiO mixed metal oxide the energy band gap of the semiconductor decreases (Table 4.2.1).

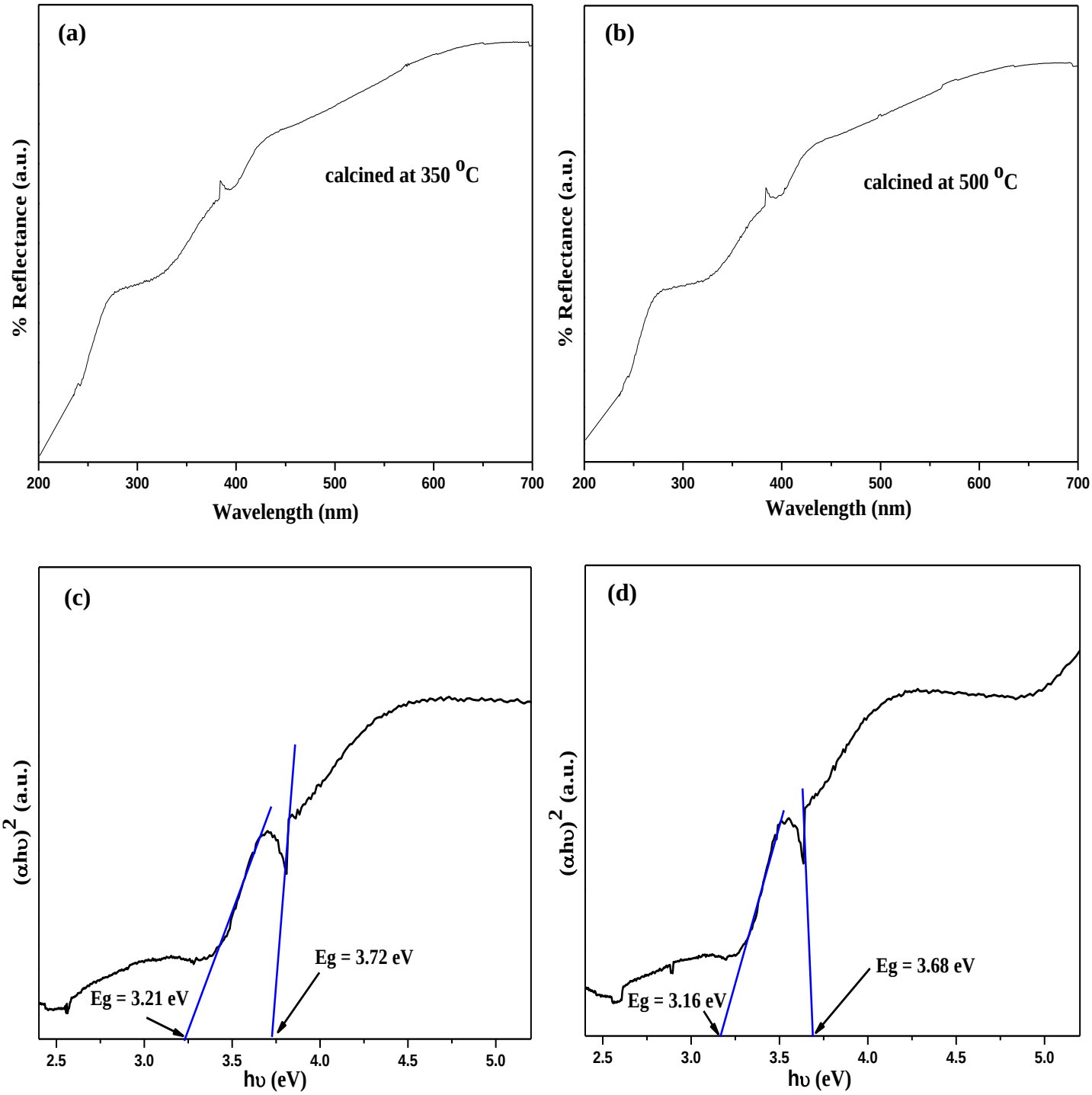


**Figure 4.2.4.** Diffuse reflectance spectra of nanocrystalline ZnO–NiO mixed metal oxide: (a) after calcination at 350 °C, (b) after calcination at 500 °C, and the plot (c) and (d) for $(\alpha h\upsilon)^2$ versus hυ drawn from the data (a) and (b).

**Table 4.2.1.** Crystallite size and band gap values of ZnO and NiO in nanocrystalline ZnO–NiO mixed metal oxide calcined at 350 $^{o}$C and 500 $^{o}$C.

| Sample | Metal oxide | Crystallite size (nm) | Band gap energy (eV) |
|---|---|---|---|
| ZnO–NiO (calcined at 350 $^{o}$C) | ZnO | 6.8 | 3.21 |
| | NiO | 8.2 | 3.72 |
| ZnO–NiO (calcined at 500 $^{o}$C) | ZnO | 27.0 | 3.16 |
| | NiO | 11.3 | 3.68 |

Surface area measurements (BET) were carried out for the as-prepared and calcined samples (Table 4.2.2). The BET results indicate that nanocrystalline ZnO–NiO mixed metal oxide calcined at 350 $^{o}$C has high specific surface area (92.8 $m^2g^{-1}$) compared to the as-prepared (SSA ~ 81.7 $m^2g^{-1}$) and calcined sample at 500 $^{o}$C (SSA ~ 77.4 $m^2g^{-1}$). The specific surface area of nanocrystalline ZnO–NiO mixed metal oxide synthesized by other methods like the impregnation [Belhadi *et al.* (2011)] and chemical precipitation [Kovalenkoa *et al.* (2008)] are lower (2 $m^2g^{-1}$ and 35 $m^2g^{-1}$ respectively) than those obtained in the present work.

**Table 4.2.2.** BET surface area of the samples before and after calcination.

| Sample | Surface area ($m^2$ $g^{-1}$) |
|---|---|
| As-prepared | 81.7 |
| ZnO–NiO (calcined at 350 $^{o}$C) | 92.8 |
| ZnO–NiO (calcined at 500 $^{o}$C) | 77.4 |

SEM images of the as-prepared and calcined (350 $^{o}$C and 500 $^{o}$C) samples show agglomeration of nanoparticles (Figures 4.2.5(a)-(c)). The EDX analyses result indicate the presence of zinc, nickel and oxygen elements in the as-prepared and calcined nanocrystalline ZnO–NiO mixed metal oxide (Figure 4.2.5(d)).

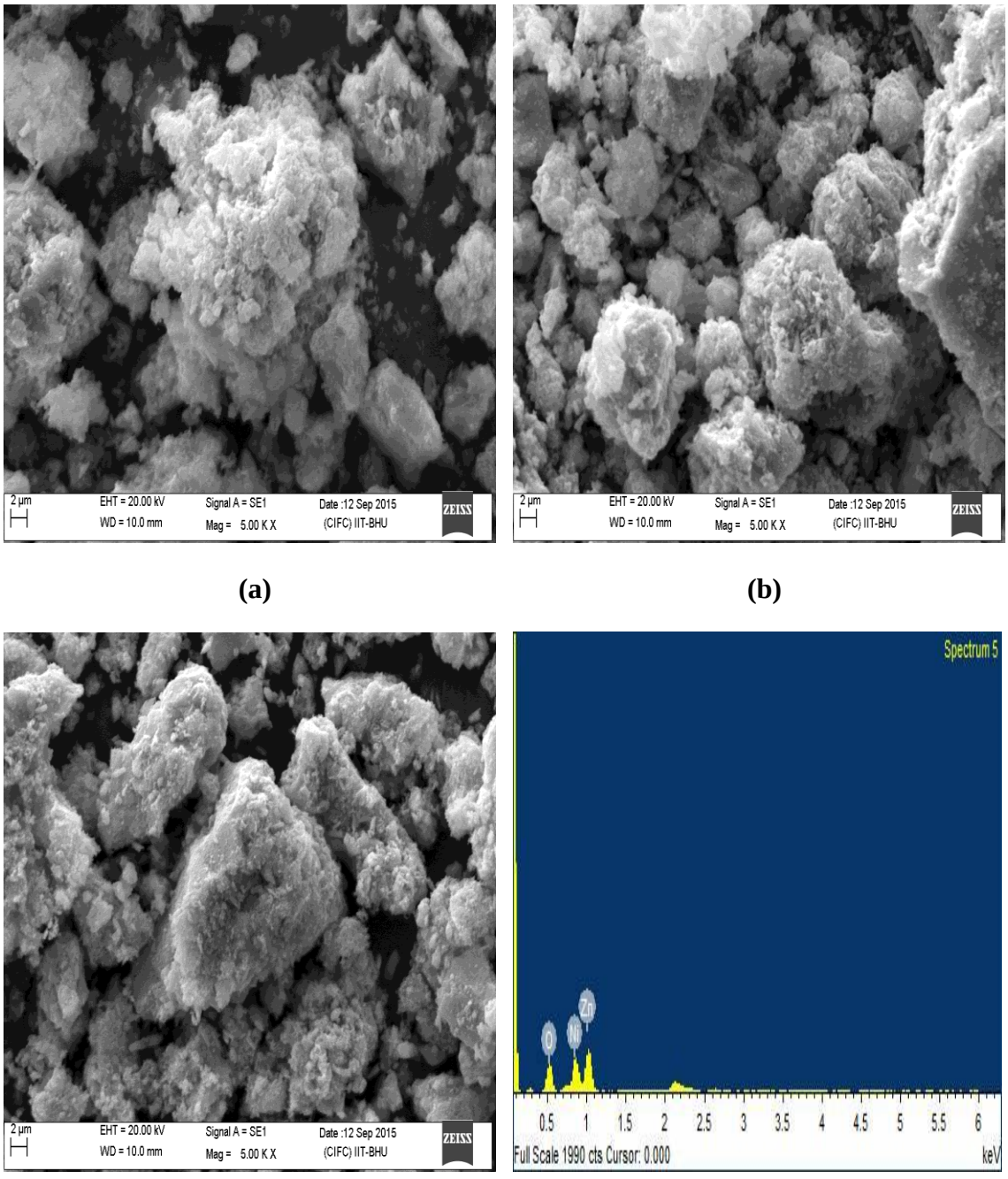


**Figure 4.2.5.** SEM images of samples (a) as-prepared, (b) calcined at 350 $^{o}$C, (c) calcined at 500 $^{o}$C, and (d) EDX analysis plot of nanocrystalline ZnO–NiO mixed metal oxide.

The EDX analysis data show almost uniform distribution of zinc, nickel and oxygen elements through the whole nanocrystalline mixed metal oxide structure.

Figure 4.2.6(a) shows TEM image of the ZnO–NiO mixed metal oxide nanoparticles after calcination at 350 $^{o}$C. The corresponding selected-area electron diffraction (SAED) pattern (Figure 4.2.6(b)) of the nanocrystalline mixed metal oxide showed clear ring pattern indicating that the sample is polycrystalline in nature. The nanocrystalline mixed metal oxide exhibits mean particle size in the range 8.5 nm–10.3 nm.

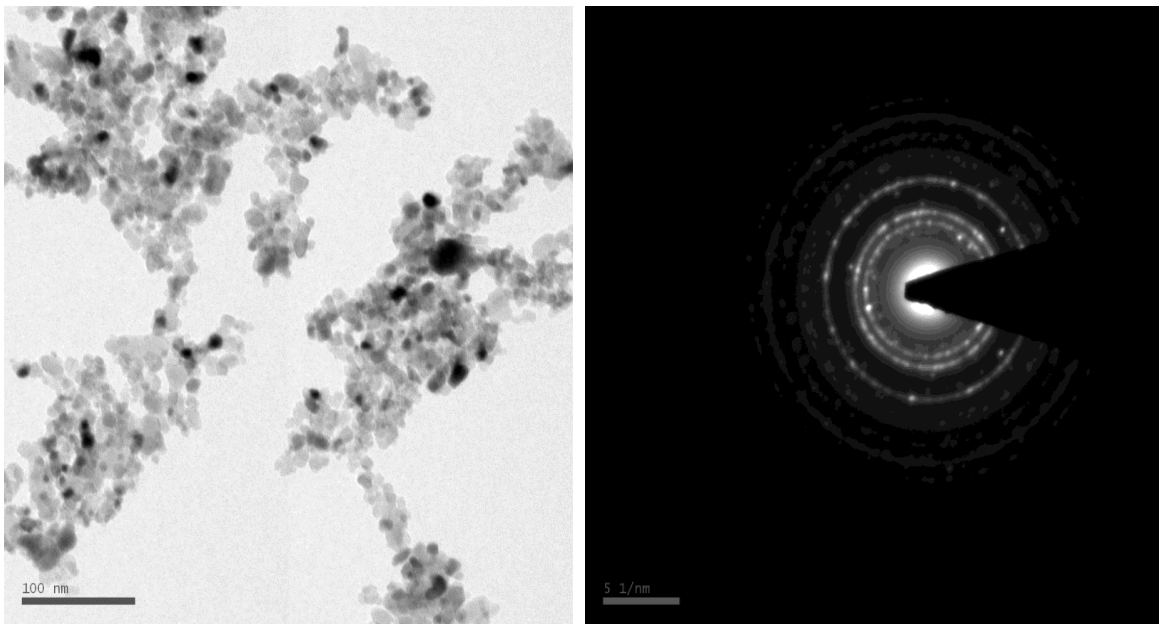


**(a)** **(b)**

**Figure 4.2.6.** (a) TEM image and (b) corresponding SAED pattern of nanocrystalline ZnO–NiO mixed metal oxide.

Figure 4.2.7 shows the magnetization versus magnetic field measurements *(M* vs. *H*) at 300 K and 10 K for nanocrystalline ZnO–NiO mixed metal oxide. The *M* versus *H* curve for the sample at 300 K indicates that the magnetic interaction is of paramagnetic nature. In this case magnetic saturation is not obtained up to field strength of 70 KOe suggesting progressive spin alignment along the external field. While *M* versus *H* curve for the sample at 10 K shows that the magnetic interaction is of ferromagnetic nature. The observed values of remanent magnetization (*Mr*) and coercivity (*Hc*) for nanocrystalline

ZnO–NiO mixed metal oxide at 10 K are 0.24 emu $g^{-1}$ and 1724 Oe respectively. Here it is worthy to note that spontaneous spin alignment occurs at low temperature in the external field. The hysteresis loop measured at 10 K is shifted towards negative field (see the inset in Figure 4.2.7) with a small exchange anisotropy of $H_{ex}$ = –21 Oe. This shows presence of uncompensated spins at the interface of the sample in frozen state [Jana *et al.* (2015)]. Figure 4.2.8 represents the magnetization versus temperature variation, i.e., *M*–*T* of the nanocrystalline ZnO–NiO mixed metal oxide. It is known that bare ZnO has no magnetic character while the bulk NiO is antiferromagnetic with a Neel temperature of 520 K [Nogues and Schuller (1999)]. However, in the nanocrystalline form NiO shows weak ferromagnetic or superparamagnetic behavior at low temperatures [Richardson and Milligan (1956), Kodama *et al.* (1997)]. The magnetic property of the nanocrystalline ZnO–NiO mixed metal oxide is obtained by monitoring the *M*–*T* behavior at field cooled (FC) and zero field cooled (ZFC) conditions and observing the magnetic transition. In the mixed metal oxide the lines of magnetization zero field cooled ($M_{ZFC}$) and magnetization field cooled ($M_{FC}$) are separated at most of the temperature region in the *M*–*T* characteristic. Nanocrystalline ZnO–NiO mixed metal oxide show the blocking temperature ($T_B$) at about 60 K in the ZFC curve (Figure 4.2.8). This corresponds to the magnetic transition in the nanocrystalline ZnO–NiO mixed metal oxide. In general, $T_B$ decreases with size of the nanoparticles because the energy barrier separating the low energy states is proportional to volume of the particles [Makhlouf *et al.* (2008)]. In nanocrystalline mixed metal oxide $M_{ZFC}$ data is decreasing from 2 K to 20 K. At the low thermal energy (< 20 K) uncompensated spins of mixed metal oxide surface makes it behave similar to ferromagnetic spins and they can spontaneously be aligned by the external magnetic field.

The most interesting observation for the nanocrystalline ZnO–NiO mixed metal oxide is that nearly at 20 K $M_{ZFC}$ data start to increase rapidly with increment in temperature up to $T_B$ (60 K). The rapid increment in the magnetic moment of the material at this temperature may be attributed to the interface effect of the mixed metal oxide [Picozzia *et al.* (2003), Chakrabarti *et al.* (2013)].

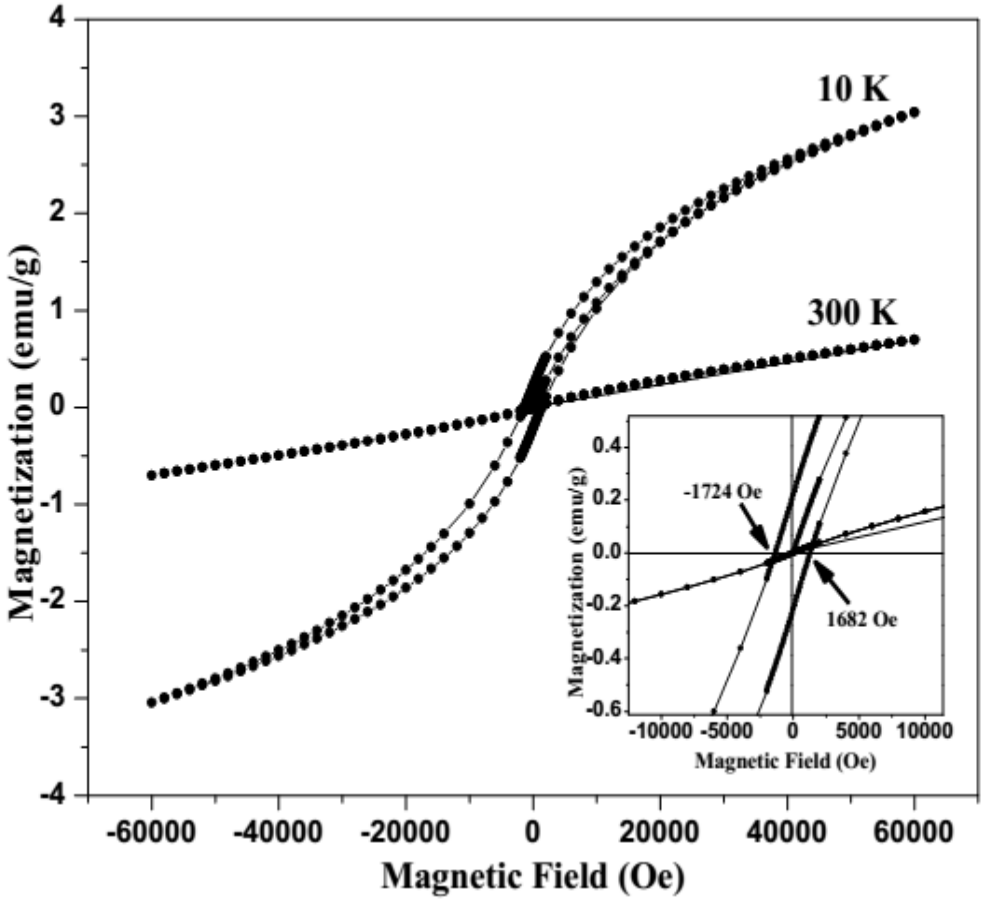


**Figure 4.2.7.** Field-dependent magnetization (*M–H*) curves recorded at 10 K and 300 K for nanocrystalline ZnO–NiO mixed metal oxide.

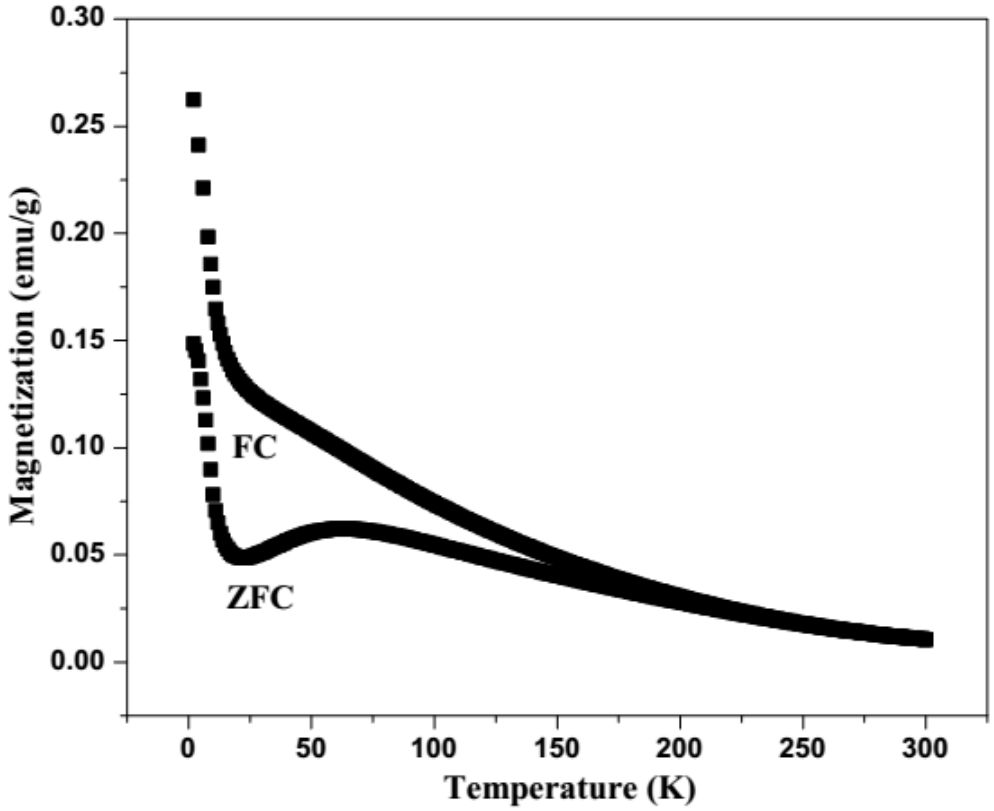


**Figure 4.2.8.** ZFC and FC curves for nanocrystalline ZnO–NiO mixed metal oxide.

In the present work, the catalytic activity of the prepared samples were also tested for the reduction of 4-nitrophenol to 4-aminophenol using sodium borohydride as reducing agent at room temperature. An aqueous solution of 4-nitrophenol is yellow in color due to the presence of nitrophenolate ions [Bayal and Jeevanandam (2012b)]. These ions on reduction with $NaBH_4$ form 4-aminophenolate ions which are colorless. The rate of catalytic reduction depends on the concentration of reagents, temperature and surface area of the catalyst. It is also well known that the rate of reaction depends on the size and shape of the nanoparticles [Mahmoud *et al.* (2010)]. The time required for the complete reduction of 4-nitrophenol to 4-aminophenol as observed by the decolorization of yellow colour in the presence of catalysts (synthesized samples) are reported in Table 4.2.3. It is inferred from Table 4.2.3 that the reduction of 4-nitrophenol does not take place in the absence of the catalyst.

On the other hand, the reduction of 4-nitrophenol does not occur when as-prepared sample was used as a catalyst. The nanocrystalline ZnO–NiO mixed metal oxide took 16–19 min for reducing the 4-nitrophenol solution. The proposed reduction mechanism of 4-nitrophenol involves the following steps [Sharma and Jeevanandam (2013), Mandlimath and Gopal (2011), Solanki and Murthy (2011)]. In the first step, 4-nitrophenolate and $BH_4^-$ ions are adsorbed onto the surface of the catalyst by chemical interaction (chemisorption). In the second step, the catalyst mediates the transfer of electrons from the donor species ($BH_4^-$ ions) to the acceptor species ($NO_2$ group) to form 4-aminophenolate ions. Desorption of the 4-aminophenolate ions occurs instantly from the catalyst surface.

**Table 4.2.3.** Time required for the complete reduction of 4-nitrophenol in the presence of synthesized samples as catalysts.

| S. No. | Reaction condition | Time required for the reduction (min) |
|---|---|---|
| 1. | 4-Nitrophenol + $NaBH_4$ | No reduction |
| 2. | 4-Nitrophenol + $NaBH_4$ + as-prepared sample | No reduction |
| 3. | 4-Nitrophenol + $NaBH_4$ + ZnO–NiO calcined at 350 $^oC$ | 16 |
| 4. | 4-Nitrophenol + $NaBH_4$ + ZnO–NiO calcined at 500 $^oC$ | 19 |

## 4.3. $Co_3O_4$–ZnO mixed metal oxide nanoparticles

### 4.3.1. Introduction

By upcoming of nano-materials a remarkable effort has been made for investigating on their significant properties which improve their use in many scientific fields. $Co_3O_4$ nanoparticles are of great importance due to their interesting electronic, electrical, optical, photochemical and magnetic properties [Makhlouf *et al.* (2013), Barakat *et al.* (2008),

Makhlouf (2002), Grzelczak *et al.* (2013)]. They are extensively used in numerous areas such as catalysts, adsorbents, gas sensors, electrochromic devices, lithium ion batteries, supercapacitors, energy storage devices, solar-selective absorbers, drug delivery, biodiagnostics and magnetic recording media [Barakat *et al.* (2008), Dong *et al.* (2007), Ma *et al.* (2014), Pacheco *et al.* (2006), Matsuda *et al.* (2015), Wang *et al.* (2009)]. $Co_3O_4$ is a magnetic p-type semiconductor with a direct optical band gaps of 1.48 and 2.19 eV [Nguyen and Shim (2015)], while ZnO is an n-type semiconductor with a wide direct band-gap (3.3–3.6 eV) and has high exciton binding energy of 60 mV at room temperature [Darezereshki *et al.* (2011)]. Due to this ZnO nanoparticles are being used in transparent conductive coatings, light-emitting diodes, hydrogen storage devices, varistor and UV lasers [Soofivand *et al.* (2013), Jia *et al.* (2008), Yildirim and Durucan (2010), Yakuphanoglu (2010)]. The superior functional performances like photocatalytic, optoelectronic and gas sensing of $Co_3O_4$–ZnO mixed metal oxide nanoparticles in comparison to the corresponding single-phase semiconductor oxides are mostly attributed to the build-up of an inner electric field at the p/n junction interface and enhanced separation of electron/hole carriers [Bekermann *et al.* (2012a), Z. Zhang *et al.* (2010), Na *et al.* (2011), Zhuge *et al.* (2010)]. The diode fabricated using p-type $Co_3O_4$ nanoplate/n-type ZnO nanorods showed reasonable electrical performance [Lee *et al.* (2012)]. The catalytic behavior was observed by the synthesized $Co_3O_4$/ZnO systems in the production of glycerol carbonate [Marcos *et al.* (2010)], catalytic oxidation of CO by $O_2$ [Shobaky and Ghozza (2004)] and low-temperature $N_2O$ decomposition reaction [Grzybek *et al.* (2015)]. The $Co_3O_4$/ZnO core/shell nanorods exhibit enhancement of photocatalytic activity in degradation of methylene blue than single $Co_3O_4$ nanorods component [Dong *et al.* (2015)]. They are also indicating attractive performances in the detection of flammable/toxic analytes ($CH_3CH_2OH$, $CH_3COCH_3$, $NO_2$) [Bekermann *et al.* (2012a), Na

*et al.* (2011)]. Hu *et al*. (2015) have reported high power $Co_3O_4$/ZnO p–n type piezoelectric transducer which can be operated at low frequencies. Kandjani *et al.* (2010) have explored the optical and magnetic properties of $Co_3O_4$–ZnO nanoparticles. According to the earlier research, the physicochemical properties of the $Co_3O_4$-based materials are generally affected by their morphologies, structures, chemical composition and sizes [Li *et al*. (2015), Zhou *et al.* (2015)]. For the synthesis of mixed metal oxide nanoparticles, various methods such as, electrochemical [Galindo *et al.* (2012)], inverse microemulsion [Gan *et al.* (1996)], hydrothermal [Kim *et al.* (2012)], solvothermal [Pang *et al.* (2015)], thermal decomposition [Zhao *et al.* (2010)], electrospinning [Moon *et al.* (2009)], microwave-assisted [Gu *et al.* (2014)], high energy mechanical ball milling [Kakazey *et al.* (2014)], thermal evaporation [Chrissanthopoulos *et al.* (2011)] and sol-gel [Amini and Rezaei (2015)] processes have been employed. However, most of these approaches generally require high reaction temperature, tedious procedures, high-energy, long reaction time, expensive equipments, and harmful organic reagents or surfactants, which might further hinder their application. Among many methods developed for the synthesis of mixed metal oxide nanoparticles the homogeneous precipitation method is the most convenient and useful technique because it not only enables to avoid complicated processes, special instruments and severe preparation conditions but also provides easy control of particle size and shape [Zhang *et al.* (2005)].

The plasma enhanced-chemical vapor deposition process used by Bekermann *et al.* (2012b) needs Ar and $O_2$ as plasma sources for the synthesis of $Co_3O_4$–ZnO nanoparticles. Dong *et al.* (2015) prepared the nanoparticles by hydrothermal method using dimethylformamide (DMF) with longer reaction time (12 h) while Jana *et al.* (2015) have employed the surfactant triethanolamine (TEA) for its preparation by a chemical route. Kanjwal *et al.* (2011) required poly vinyl alcohol (PVA), a high-voltage power

supply (source of the electric field) and longer time (24 h) in an electrospinning process followed by a hydrothermal technique. Zhang *et al.* (2015) have used polyvinyl pyrrolidone (PVP), ethylene glycol (EG) and teflon-lined stainless steel autoclave in a solvothermal method. In the present work $Co_3O_4$–ZnO mixed metal oxide nanoparticles with high purity has been synthesized by homogeneous precipitation method which is a simple, inexpensive, environmentally friendly without using any organic additive or surfactant and samples were prepared at low temperature in short time in large scale production. After thorough characterization, optical and magnetic properties of the nanoparticles were also investigated.

### 4.3.2. Experimental

(i) Materials

The chemicals used were cobalt (II) oxalate dihydrate ($CoC_2O_4 \cdot 2H_2O$) (SIGMA ALDRICH®), zinc (II) acetate dihydrate ($Zn(CH_3COO)_2 \cdot 2H_2O$) (MERCK®) and ammonia solution (25%, RANKEM®). All the chemicals were analytical grade and were used as reagents as received without further purification. The solutions were prepared in Millipore® water.

(ii) Synthesis

In the present study, $Co_3O_4$–ZnO mixed metal oxide nanoparticles were prepared through proper precursors by a surfactant-free homogeneous precipitation method. The synthetic details are as follows.

In a 250 mL beaker 90 mL aqueous solution of cobalt oxalate (8 mmol) and 90 mL aqueous solution of zinc acetate (8 mmol) were taken. Subsequently, 14 mL of 25% aqueous ammonia solution (ammonium hydroxide) was added dropwise into the above mixture and the contents were heated to ~ 80 $^oC$ with continuous stirring for 2 h. During the reaction a light pink precipitate formed which was filtered off, washed first with water

four times to remove any impurity, then with ethyl alcohol two times and dried in an oven at 75 $^{o}$C. The as prepared sample was grounded to fine powder with the help of a mortar and pestle. Finally calcination of the as-prepared powder was carried out in air at 350 $^{o}$C and 500 $^{o}$C at a heating rate of 2 $^{o}$C/min for 3 h inside a muffle furnace. The colors of the samples before and after calcination were light pink and black respectively.

### 4.3.3. Results and discussion

Appropriate amount of ammonium hydroxide was added to a mixture of aqueous cobalt oxalate and aqueous zinc acetate solution with continuous stirring for 2 h at about 80 $^{o}$ C and the following reactions take place:

$$6CoC_2O_4 \cdot 2H_2O\ (aq.) + 6Zn(CH_3COO)_2 \cdot 2H_2O\ (aq.) + 24NH_4OH\ (aq.) \rightarrow$$
$$3Zn(OH)_2 + 3Zn(CH_3COO)_2(NH_3)_2 + 3Co(OH)_2 + Co_3O_4 + 6(NH_4)_2C_2O_4 +$$
$$6CH_3COONH_4 + 32H_2O + H_2\ (g) \qquad (4.3.1)$$

After calcination

$$Zn(CH_3COO)_2(NH_3)_2 + [O] \rightarrow ZnO + C_2H_6\ (g) + 2CO_2\ (g) + 2NH_3\ (g) \qquad (4.3.2)$$

$$Zn(OH)_2 \rightarrow ZnO + H_2O \qquad (4.3.3)$$

$$3Co(OH)_2 \rightarrow Co_3O_4 + 2H_2O + H_2\ (g) \qquad (4.3.4)$$

After calcination the formation of pure $Co_3O_4$–ZnO mixed metal oxide nanoparticles is evidenced by the XRD data.

The X-ray powder diffraction results of the as-prepared and calcined (350 $^{o}$C and 500 $^{o}$C) samples are shown in Figure 4.3.1. XRD pattern of the as-prepared sample shows four phases: one due to β-$Zn(OH)_2$ (JCPDS file no. 20-1435), second due to zinc acetate ammonia ($Zn(CH_3COO)_2(NH_3)_2$) (JCPDS file no. 21-1468), third due to β-$Co(OH)_2$ (JCPDS file no. 51-1731) and the fourth due to $Co_3O_4$. After calcination at 350 $^{o}$C and 500 $^{o}$C diffraction peaks were observed at $2\theta \approx 18.97^{o}$, $31.32^{o}$, $36.87^{o}$, $38.58^{o}$, $44.89^{o}$, $55.64^{o}$, $59.40^{o}$ and $65.25^{o}$ which are indexed at diffraction lines of (111), (220), (311),

(222), (400), (422), (511) and (440) respectively corresponding to typical cubic spinel structure $Co_3O_4$ which is in good agreement with JCPDS No. 42–1467. In the same XRD pattern diffraction peaks of hexagonal ZnO with lattice parameters of $a$ = 0.3250 nm and $c$ = 0.5207 nm were also obtained at $2\theta \approx 34.36^o$, $56.58^o$, $62.87^o$, $67.91^o$, $69.0^o$, $72.68^o$ and $76.89^o$ which are indexed to the (002), (110), (103), (112), (201), (004) and (202) diffraction lines respectively (JCPDS file no. 79-2205). The XRD patterns confirm the formation of pure $Co_3O_4$–ZnO mixed metal oxide after calcination. The crystallite sizes of the calcined samples were calculated by means of the Debye-Scherrer equation.

The crystallite size of $Co_3O_4$ is 8.3 nm in the sample calcined at 350 $^oC$ while it is 12.7 nm in the sample calcined at 500 $^oC$. It is found from the XRD analyses that on increasing calcination temperature the intensity of the diffraction peaks also increase which is ascribed to the larger crystallite size.

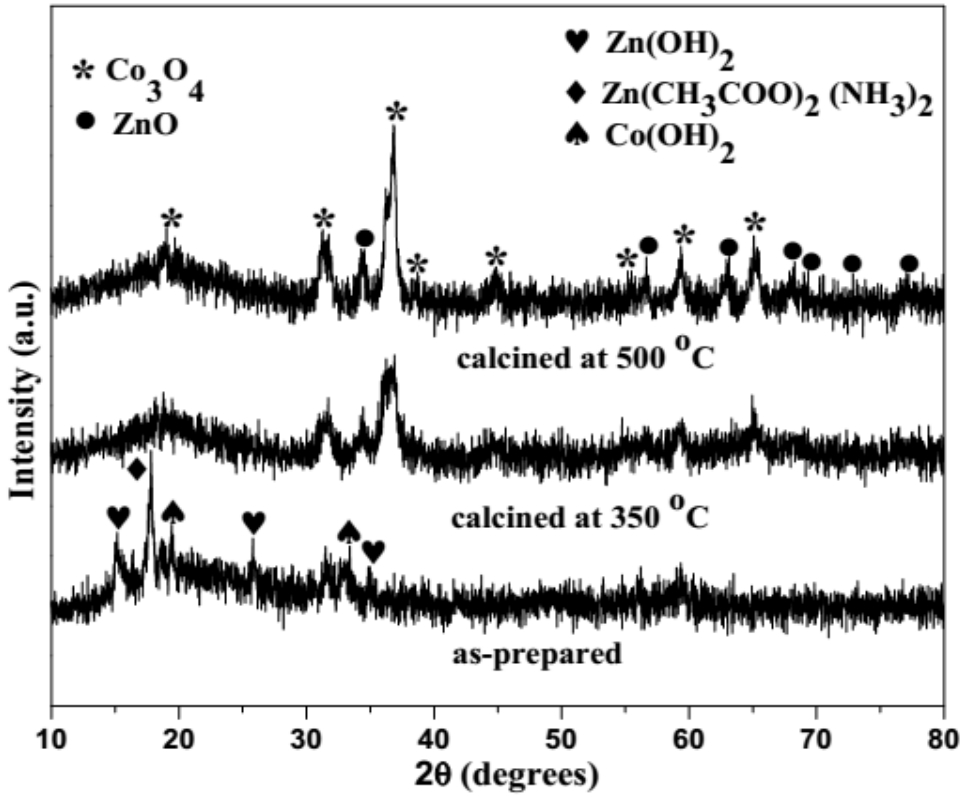


**Figure 4.3.1.** XRD patterns of the as-prepared and calcined samples at 350 $^o$ and 500 $^oC$.

The thermal gravimetric analysis pattern for as-prepared powder is shown in Figure 4.3.2. The overall weight losses (about 39.4 %) between 25-350 $^{o}$C are attributed to the dehydration of metal hydroxide to metal oxide and also to the removal of inorganic and organic matters obtained from the decomposition of zinc acetate ammonia [Wang *et al.* (2011), Kim *et al.* (2010)]. There is no weight loss after 350 $^{o}$C confirming the formation of $Co_3O_4$–ZnO mixed metal oxide.

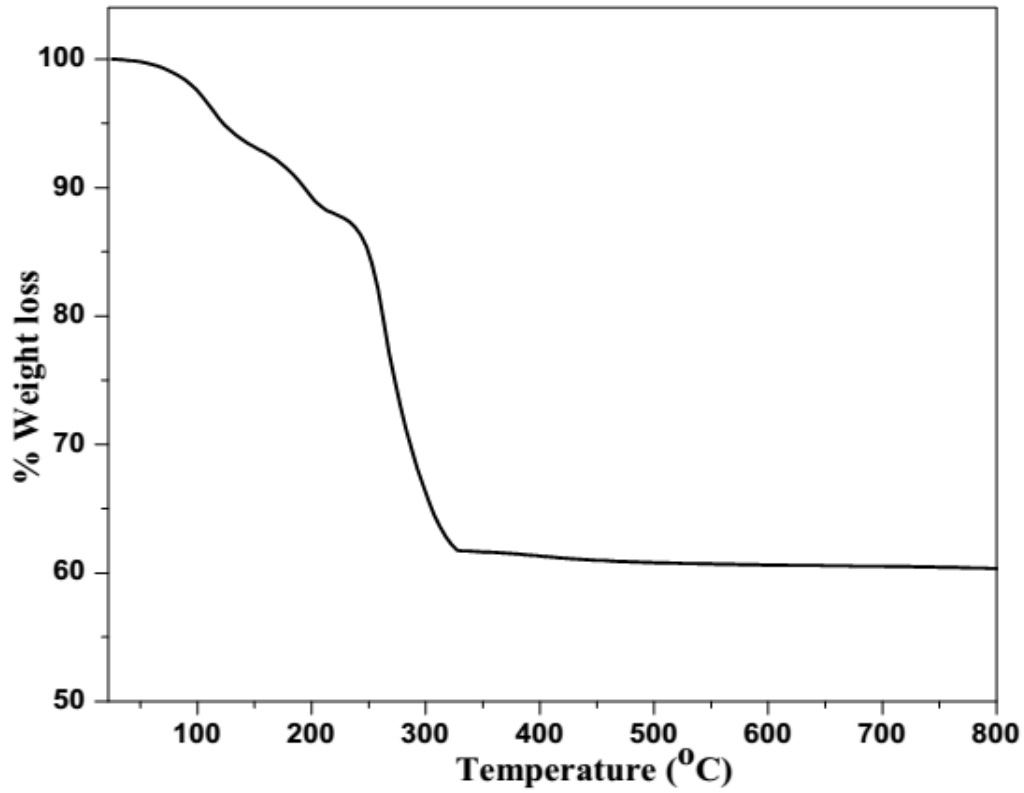


**Figure 4.3.2.** Thermal gravimetric analysis curves of the as-prepared sample.

The FT-IR spectra of as-prepared and calcined (350 $^{o}$C and 500 $^{o}$C) samples are presented in Figure 4.3.3. The broad band at around 3545–3357 cm$^{-1}$ in the spectra of as-prepared sample is ascribed to the stretching vibrations of –OH and –NH which does not appear in the calcined sample [Cheng *et al.* (2014)]. The band at about 2930 cm$^{-1}$ is attributed to C–H stretching in the spectra of the as-prepared sample [Sharma and Jeevanandam (2013)]. In the spectrum of the as-prepared sample the bands at 1330 and 1625 cm$^{-1}$ are assigned to the binding of acetate ion to zinc (II) and these disappear in case of calcined samples

[Wang *et al.* (2011)]. The band at 1249 $cm^{-1}$ is due to –C–O stretching in the spectra of as-prepared sample. The bands at 490 and 777 $cm^{-1}$ are associated with Co-O stretching and Co-OH bending vibrations in the spectra of the as-prepared sample [Contreras *et al.* (2010)]. The bands appearing at about 565 ($\nu_1$) and 664 ($\nu_2$) $cm^{-1}$ originate from the stretching vibrations of the Co–O bonds in the spectra of calcined samples [Niasari *et al*. (2009a)]. The $\nu_1$ band is due to $Co^{3+}$–O vibration in the octahedral hole and $\nu_2$ band is a characteristic of $Co^{2+}$–O vibration in tetrahedral hole in the spinel lattice [Wang *et al.* (2010)]. The lower frequency band at 468 $cm^{-1}$ is attributed to the Zn-O stretching vibrations in the spectra of the calcined samples [Thangaraj *et al.* (2011)].

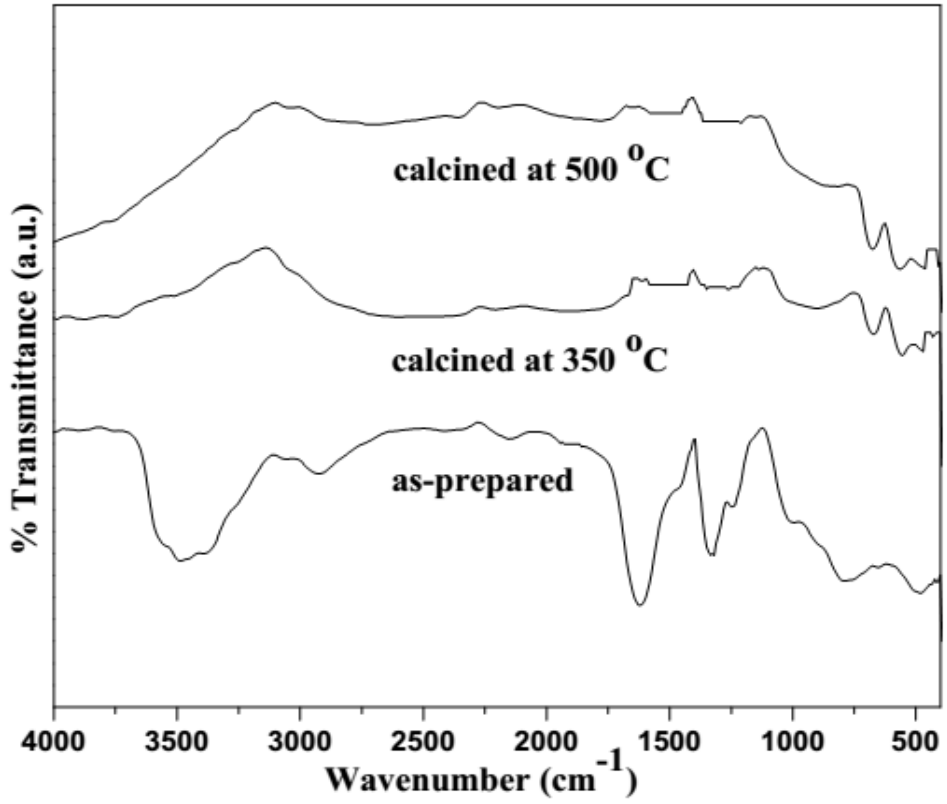


**Figure 4.3.3.** FT-IR spectra of the as-prepared and calcined samples at 350 $^{o}$ and 500 $^{o}$C.

X-ray photoelectron spectroscopy (XPS) is a quantitative spectroscopic method that determines the chemical-states of the elements present in the materials. The XPS spectra of Co 2p, Zn 2p, and O 1s in $Co_3O_4$–ZnO mixed metal oxide nanoparticles are shown in Figure 4.3.4(a). The peaks of Co $2p_{3/2}$ and Co $2p_{1/2}$ correspond to the binding energy of

780.3 eV and 795.7 eV respectively (Figure 4.3.4(b)) which matches with the binding energy of $Co_3O_4$ of the earlier work [Tak and Yong (2008)]. In Figure 4.3.4(c), the binding energy for spin orbit doublet peaks of the Zn $2p_{3/2}$ and Zn $2p_{1/2}$ in ZnO appeared at about 1021.7 eV and 1045.2 eV respectively which are consistent with other reports [Lupan *et al.* (2010)]. Two peaks are clearly marked at 529.9 eV and 531.3 eV for O 1s spectrum of the $Co_3O_4$–ZnO mixed metal oxide nanoparticles (Figure 4.3.4(d)). The main low-energy oxygen peak at 529.9 eV is assigned to the lattice oxygen ($O^{2-}$) present in the $Co_3O_4$–ZnO mixed metal oxide nanoparticles [Dong *et al.* (2015)]. The second peak at higher binding energy (531.3 eV) is similar to that reported for the surface hydroxyls and chemisorbed oxygen [Dong *et al.* (2015), McCafferty and Wightman (1998)]. The XPS analysis of the samples gives the atomic ratio of Co to Zn as 2.87 (at. % Co = 31.24 and Zn = 10.87) and 2.94 (at. % Co = 33.11 and Zn = 11.26) in the calcined samples at 350 $^oC$ and 500 $^oC$ respectively. XPS compositional analyses supported the presence of $Co_3O_4$ and ZnO in the mixed metal oxide nanoparticles. The XPS results are in good agreement with XRD measurements.

UV–visible diffuse reflectance spectroscopy is one of the most important techniques to reveal the band structure or molecular energy levels in the semiconductor materials. Diffuse reflectance spectra of the calcined samples at 350 $^oC$ and 500 $^oC$ are presented in Figures 4.3.5(a) and (b). The UV-visible spectra of the samples calcined at 350 $^oC$ and 500 $^oC$ exhibit one band at 363 nm and 374 nm, respectively. Kubelka–Munk formula [Yakuphanoglu (2010)] is used to calculate the optical absorption coefficient ($\alpha$). The optical band gap ($E_g$) of $Co_3O_4$–ZnO mixed metal oxide nanoparticles is determined by extrapolation of the linear relationship between $(\alpha h\upsilon)^2$ and $(h\upsilon)$ [Matsuda *et al.* (2015)]. The $(\alpha h\upsilon)^2$ on the y axis versus photo energy $(h\upsilon)$ on the x-axis are plotted in Figures 4.3.5(c) and (d) on the basis of data obtained from Figures 4.3.5(a) and (b). The estimated

band-gap energy, thus obtained, are ~ 3.41 and 3.31 eV for samples calcined at 350 $^{o}$C and 500 $^{o}$C respectively [Kandjani *et al.* (2010)]. Generally the optical band gap is influenced by several factors such as morphology, compositions, surface defect states (oxygen vacancies) and quantum confinement effects of the nanoparticles [Farhadi *et al.* (2013), Zak *et al.* (2011)]. The optical properties of $Co_3O_4$–ZnO mixed metal oxide nanoparticles are important for solar cells, electrochromic devices and gas sensor applications.

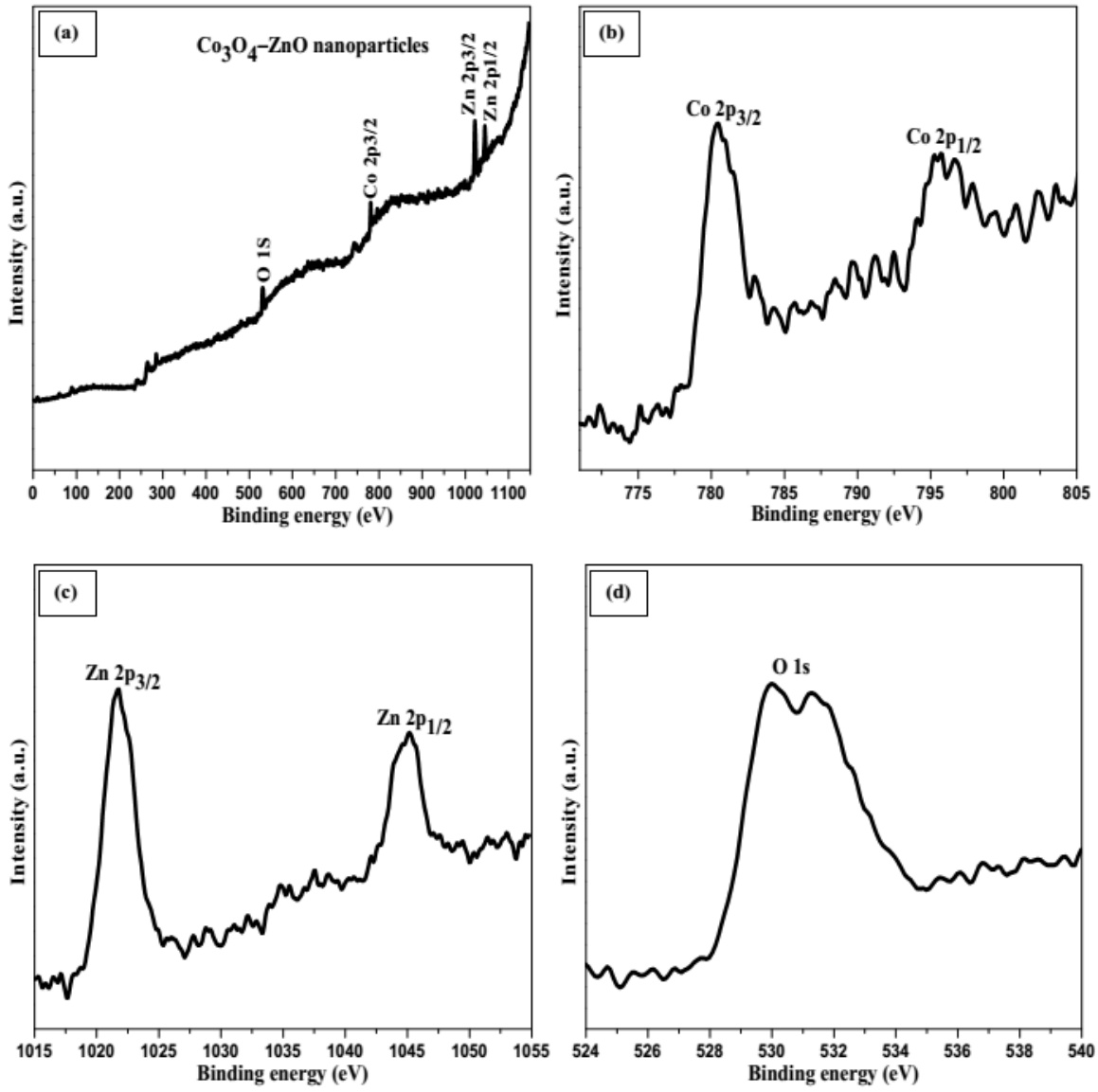


**Figure 4.3.4.** XPS spectra of (a) $Co_3O_4$–ZnO mixed metal oxide nanoparticles, (b) Co 2p, (c) Zn 2p and (d) O 1s.

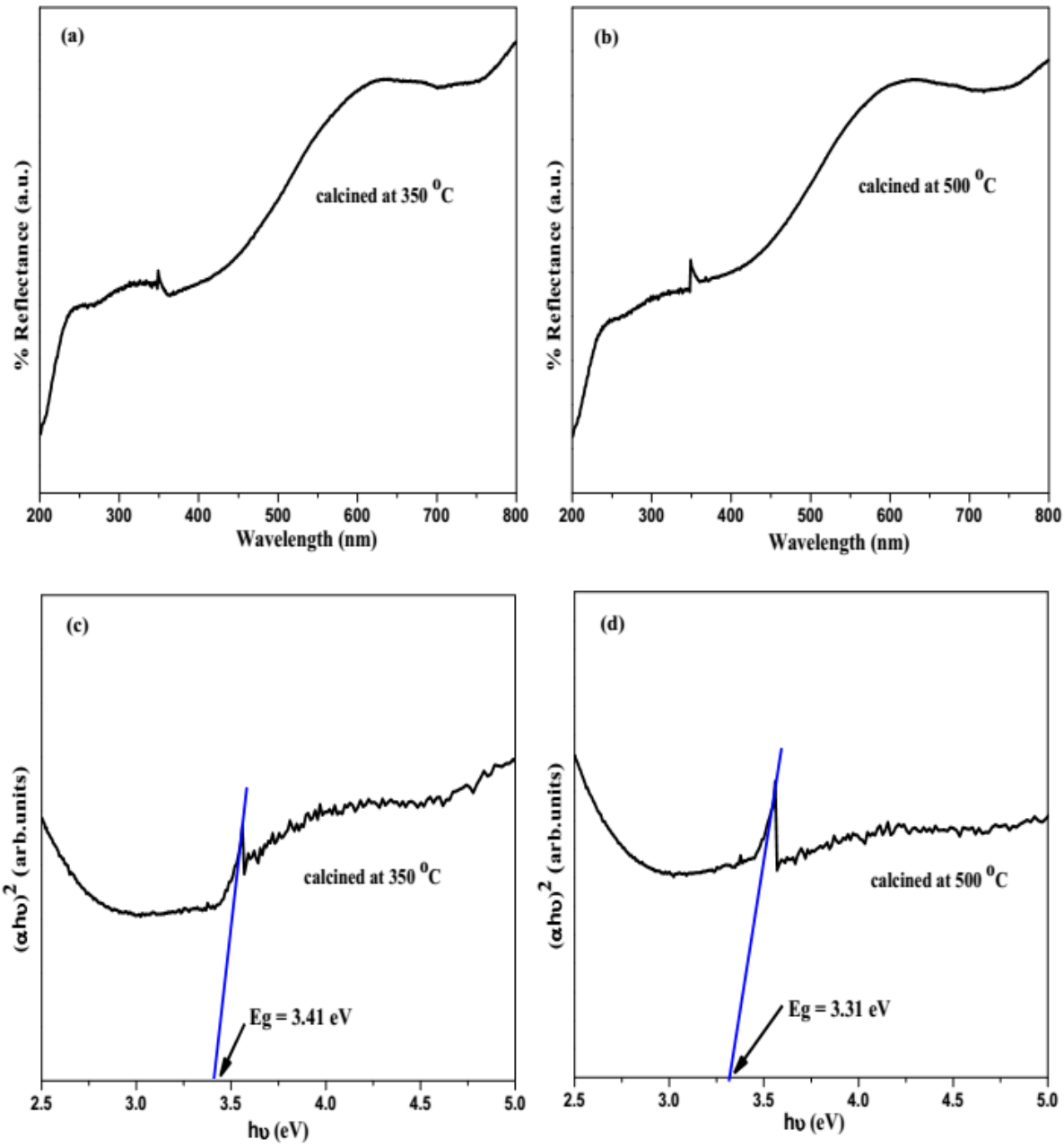


**Figure 4.3.5.** Diffuse reflectance spectra of $Co_3O_4$–ZnO mixed metal oxide nanoparticles: (a) after calcination at 350 $^oC$, (b) after calcination at 500 $^oC$, and the plots (c) and (d) for $(\alpha h\upsilon)^2$ versus $h\upsilon$ drawn from the data (a) and (b).

The specific surface area of as-prepared and calcined $Co_3O_4$–ZnO samples was measured using BET (Brunauer–Emmett–Teller) method and the results are given in Table 4.3.1. The BET results indicate that $Co_3O_4$–ZnO mixed metal oxide calcined at 350 $^oC$ has high specific surface area (72.4 $m^2g^{-1}$) in comparison to the as-prepared (SSA ~ 16.7 $m^2g^{-1}$) and calcined sample at 500 $^oC$ (SSA ~ 67.8 $m^2g^{-1}$).

The specific surface area of $Co_3O_4$–ZnO mixed metal oxide nanoparticles synthesized by other techniques like the hydrothermal [Kandjani *et al.* (2010)], solvothermal [Zhang *et al.* (2015)] and thermal decomposition [Zhu *et al.* (2015)] are significantly lower (54.6 $m^2g^{-1}$, 60.9 $m^2g^{-1}$ and 46.9 $m^2g^{-1}$ respectively) than those obtained in the present method.

**Table 4.3.1.** BET surface area of the samples before and after calcination.

| **Sample** | **Surface area ($m^2$ $g^{-1}$)** |
|---|---|
| As-prepared | 16.7 |
| $Co_3O_4$–ZnO (calcined at 350 $^oC$) | 72.4 |
| $Co_3O_4$–ZnO (calcined at 500 $^oC$) | 67.8 |

SEM images of the as-prepared and calcined samples at 350 $^oC$ and 500 $^oC$ show agglomeration of nanoparticles (Figures 4.3.6(a)-(c)). The growth mechanism of the nanoparticles explained on the basis of precipitation, dissolution, renucleation, growth, aggregation [Garakani *et al.* (2015), Thanh *et al.* (2014)]. First on supersaturation the primary precipitates were formed. This was followed by dissolution of unstable precipitates which on renucleation and growth of crystallites takes place. The resultant crystallites were aggregated or attached onto the final crystals to minimize the interfacial energy. The EDX analyses results indicate the presence of cobalt, zinc and oxygen elements in the as-prepared and calcined samples (Figure 4.3.6(d)).

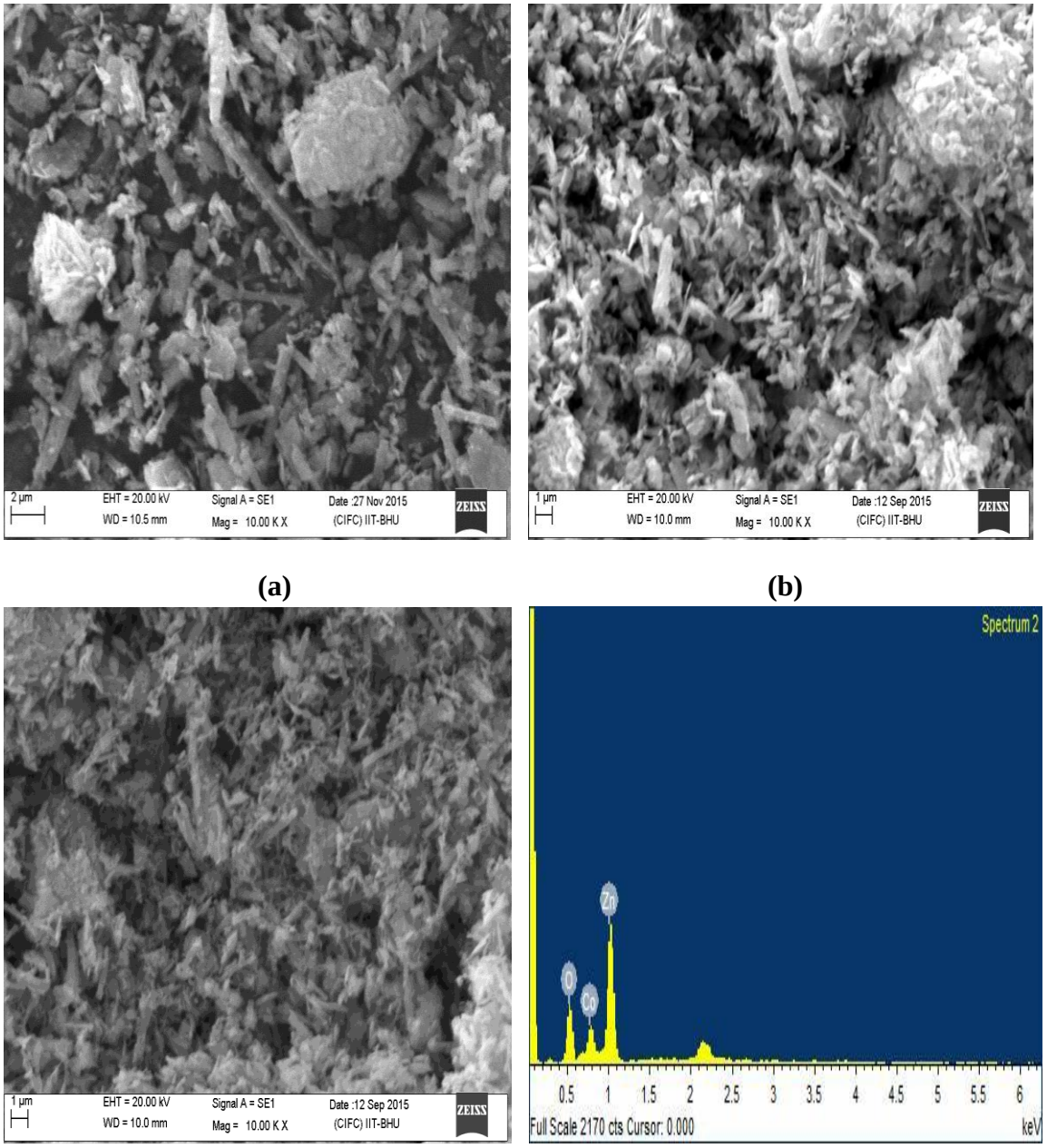


**Figure 4.3.6.** SEM images of samples (a) as-prepared, (b) calcined at 350 $^{o}$C, (c) calcined at 500 $^{o}$C, and (d) EDX analysis plot of $Co_3O_4$–ZnO mixed metal oxide nanoparticles.

The EDX analysis data of the samples give the atomic ratio of Co to Zn as 2.98 and 3.00 in the calcined samples at 350 $^{o}$C and 500 $^{o}$C respectively (Table 4.3.2) which is closely match with the XPS results. The EDX analyses data show almost uniform distribution of cobalt, zinc and oxygen elements throughout the whole mixed metal oxide nanoparticles structure.

**Table 4.3.2.** EDXA data of the calcined samples at 350 $^{o}$ and 500 $^{o}$C.

| Sample | Element | At% | Wt% | Co/Zn |
|---|---|---|---|---|
| $Co_3O_4$–ZnO (calcined at 350 $^{o}$C) | Co | 35.56 | 56.43 | 2.98 |
| | Zn | 11.92 | 20.97 | |
| | O | 52.52 | 22.60 | |
| $Co_3O_4$–ZnO (calcined at 500 $^{o}$C) | Co | 37.32 | 57.75 | 3.00 |
| | Zn | 12.44 | 21.36 | |
| | O | 49.76 | 20.89 | |

TEM images of the $Co_3O_4$–ZnO mixed metal oxide nanoparticles after calcination at 350 $^{o}$C showed in Figures 4.3.7(a) and (b). It is seen that the darker parts of the image is similar to a spherical shape, they are related to $Co_3O_4$ whereas brighter irregular-shapes are related to ZnO in sample. The corresponding selected-area electron diffraction (SAED) pattern (Figure 4.3.7(c)) of the mixed metal oxide nanoparticles showed several distinct concentric rings suggesting that the sample is polycrystalline in nature. The estimated average particle size of $Co_3O_4$ in mixed metal oxide nanoparticles is in the range 9.5–11.3 nm which is in agreement with the value calculated from XRD measurements. A pictorial model showing the mixed metal oxide nanoparticles is demonstrated in Figure 4.3.7(d).

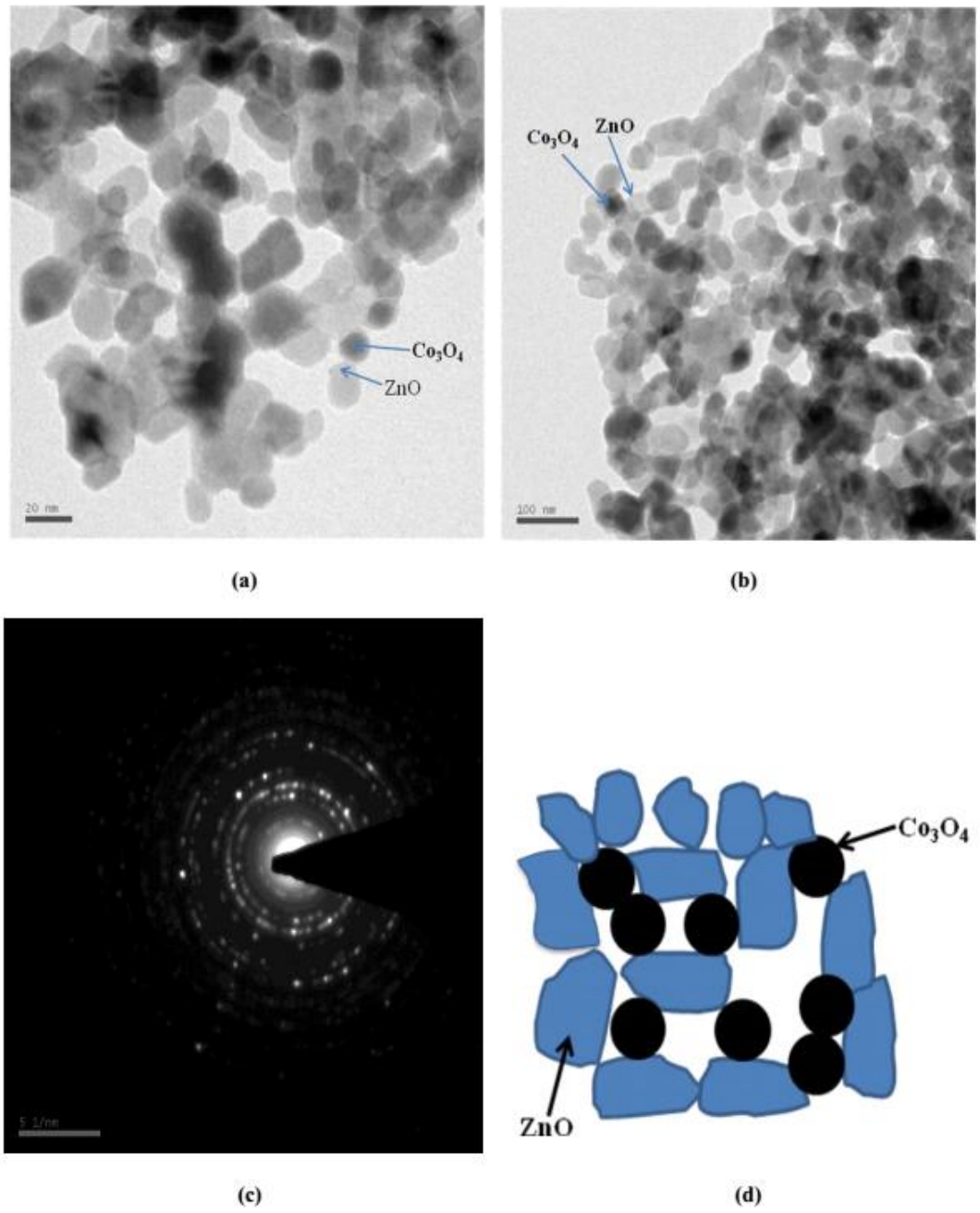


**Figure 4.3.7.** (a)-(b) TEM images, (c) corresponding SAED pattern of $Co_3O_4$–ZnO mixed metal oxide nanoparticles and (d) schematic model of the mixed metal oxide nanoparticles.

Variation in magnetization versus magnetic field measurements *(M–H)* at 300 K and 10 K for $Co_3O_4$–ZnO mixed metal oxide nanoparticles are shown in Figure 4.3.8. At 300 K *M* varies linearly with *H* up to 60 kOe implying the magnetic interaction is of paramagnetic (PM) behaviour in the mixed metal oxide sample.

In this case the magnetization is not saturated even at an applied field of 70 kOe suggesting progressive spin alignment along the external field. While the *M–H* curve for the sample at 10 K gives the fine shape to the hysteresis loop which is a characteristic of weak ferromagnetic nature. From the inset of Figure 4.3.8 the estimated remanent magnetization (*Mr*) and coercive field (*Hc*) are 0.0068 emu/g and 175 Oe respectively. The low coercive field and remanent magnetization confirm weak ferromagnetic properties for the mixed metal oxide nanoparticles. It also justifies spontaneous spin alignment by the external magnetic field in the mixed metal oxide sample at low temperature. The hysteresis loop at 10 K gets broadened and is shifted towards negative field (see the inset in Figure 4.3.8) with a small exchange anisotropy of $H_{ex}$ = –36.5 Oe. It is attributed to the presence of uncompensated spin at the interface of the sample in the frozen state. Exchange bias is the shift of the hysteresis loop along the direction of magnetic field axis. It arises from the coupling at the interface between $Co_3O_4$ antiferromagnetic core and uncompensated ferromagnetic moments at the surface [Jana *et al.* (2015)]. Exchange bias depends on different parameters such as spin orientation or anisotropy, roughness, spin configuration, magnetic domains and atomic intermixing at the interface [Nogues and Schuller (1999)]. According to the reported mechanism [Nogues *et al.* (1996)] the exchange bias effect is schematically shown in Figure 4.3.9. In the range $T_N < T < T_C$, the cooling field induces the alignment of the ferromagnetic (FM) spins along its direction (Figure 4.3.9(i)) while at $T < T_N$ the spins of the antiferromagnetic (AFM) phase arrange in an antiferromagnetic configuration (Figure 4.3.9(ii)). When the magnetic field is reversed, the FM spins have a tendency to reorient while the AFM spins remain unchanged due to the large AFM anisotropy (Figures 4.3.9(iii)-(v)). The ferromagnetic interaction at the FM-AFM interface gives a strong

restoring force on the FM spins reorientations and therefore a shift of the M-H loop is produced.

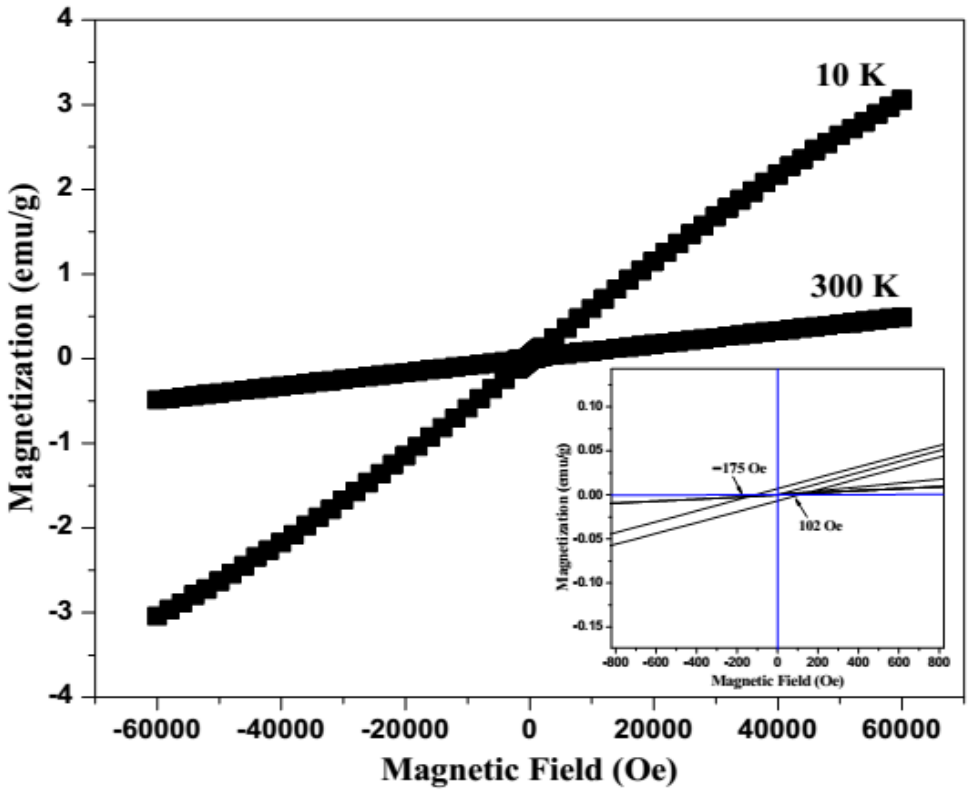


**Figure 4.3.8.** Field-dependent magnetization (*M–H*) curves recorded at 10 K and 300 K for $Co_3O_4$–ZnO mixed metal oxide nanoparticles.

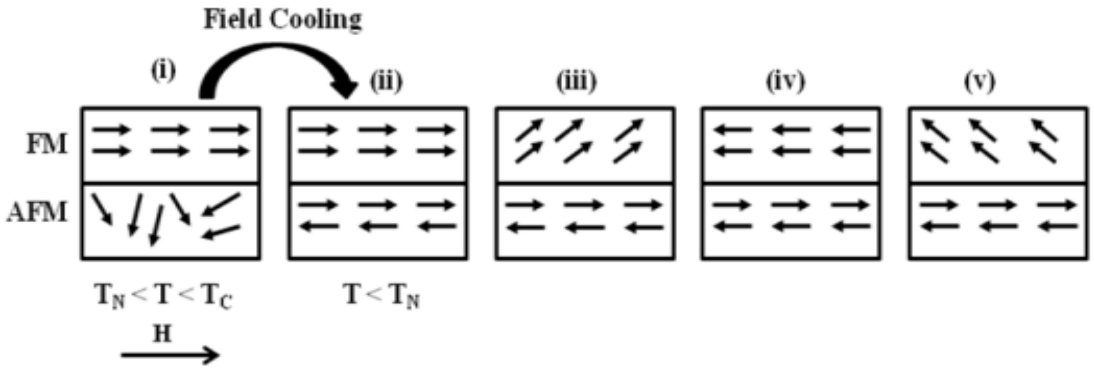


**Figure 4.3.9.** Schematic of the exchange bias mechanisms.

The temperature dependence of zero-field-cooled (ZFC) and field-cooled (FC) magnetization curves for the $Co_3O_4$–ZnO mixed metal oxide nanoparticles under an applied field of 500 Oe are presented in Figure 4.3.10. It is already known that bare ZnO

has no magnetic character, while bulk $Co_3O_4$ is an antiferromagnetic with the Neel temperature $T_N$ = 40 K [Sharma *et al.* (2012)]. For bulk antiferromagnetic materials the net magnetization is zero due to complete compensation of sublattice magnetizations. $Co_3O_4$–ZnO mixed metal oxide nanoparticles show the blocking temperature ($T_B$) at about 38 K in the curves (Figure 4.3.10) which corresponds to the magnetic transition in the mixed metal oxide nanoparticles. In the *M*–*T* characteristic curves of the sample $M_{ZFC}$ and $M_{FC}$ lines get separated below 38 K temperature. The most interesting observation for the $Co_3O_4$–ZnO mixed metal oxide nanoparticles is that on decreasing temperature both $M_{ZFC}$ and $M_{FC}$ data start to increase nearly at 38 K. The increment in the magnetic moment of the material at this low temperature is attributed to the interface effect of the mixed metal oxide nanoparticles [Jana *et al.* (2015)]. At the low thermal energy (< 38 K) uncompensated surface spins and/or finite size effects of the mixed metal oxide nanoparticles makes it behave similar to the ferromagnetic spins and they can spontaneously be aligned by the external magnetic field.

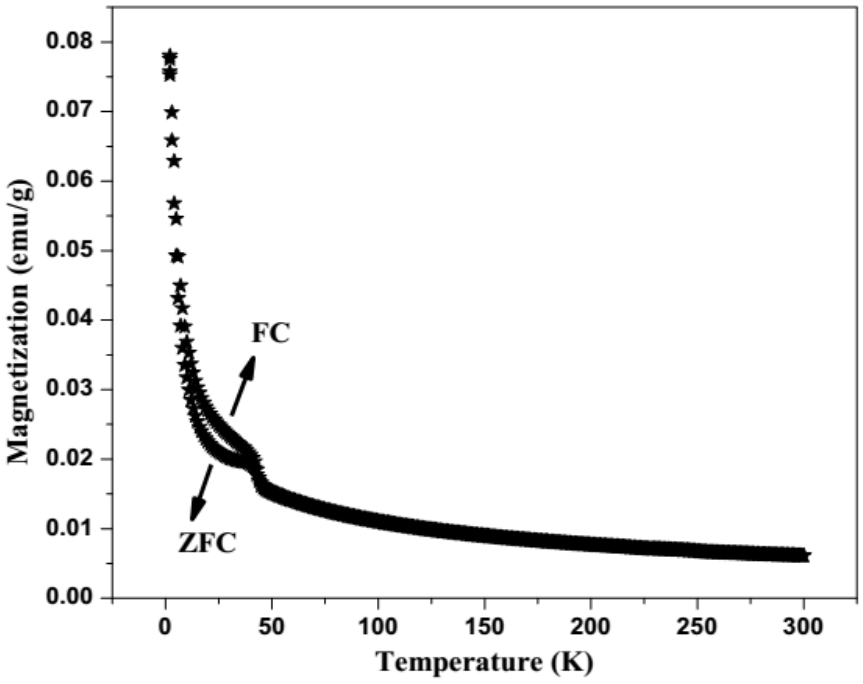


**Figure 4.3.10.** ZFC and FC curves for $Co_3O_4$–ZnO mixed metal oxide nanoparticles.

## 4.4. Conclusions

Nanocrystalline CuO–ZnO mixed metal oxide was successfully synthesized by a simple homogeneous precipitation method in short precipitation time without using any surfactant or chelating agents. The samples were characterized using an array of analytical techniques. The results show that the morphology and specific surface area of the samples are influenced by the calcination temperature. It is also observed that the specific surface area of the synthesized sample depends on its precipitation time. The current homogeneous precipitation method may be employed for the synthesis of other nanocrystalline mixed metal oxides. The catalytic ability of the powder samples is demonstrated by the conversion of 4-nitrophenol to 4-aminophenol using $NaBH_4$ at room temperature. The studies reveal that the as-prepared powder exhibits better catalytic performance compared to the calcined nanocrystalline CuO–ZnO mixed metal oxide and pure CuO nanoparticles. This catalyst could also be used in the reduction of other aromatic nitrocompounds.

The optical band gap value of ZnO and NiO in mixed metal oxide decreases on increasing the calcination temperature. The surface area measurements show high surface area for the nanocrystalline mixed metal oxide which are obtained in the present method. The nanocrystalline ZnO–NiO mixed metal oxide exhibits ferromagnetic behavior at low temperature. It also acts as a catalyst for the reduction of 4-nitrophenol to 4-aminophenol. The present synthetic approach may be extended to the preparation of other mixed metal oxide nanoparticles.

The estimated optical band-gap value are 3.41 and 3.31 eV for $Co_3O_4$–ZnO mixed metal oxide nanoparticles calcined at 350 and 500 $^oC$ respectively. The mixed metal oxide nanoparticles obtained in the present work show high surface area. This method may be extended to the preparation of other mixed metal oxide nanoparticles. The prepared

$Co_3O_4$–ZnO mixed metal oxide nanoparticles exhibit weak ferromagnetic behavior at low temperature with low coercive field (175 Oe) and remanent magnetization (0.0068 emu/g). The perspective applications of $Co_3O_4$–ZnO mixed metal oxide nanoparticles include sensing, photocatalysis and optoelectronics.